

A Catalog of H I Clouds in the Large Magellanic Cloud

S. Kim¹, E. Rosolowsky², Y. Lee³, Y. Kim¹, Y.C. Jung⁴, M.A. Dopita⁵, B.G. Elmegreen⁶, K.C. Freeman⁵, R.J. Sault⁷, M. Kesteven⁷, D. McConnell⁷, & Y.-H. Chu⁸

ABSTRACT

A 21 cm neutral hydrogen interferometric survey of the Large Magellanic Cloud (LMC) combined with the Parkes multi-beam H I single-dish survey clearly shows that the H I gas is distributed in the form of clumps or clouds. The H I clouds and clumps have been identified using a thresholding method with three separate brightness temperature thresholds (T_b). Each catalog of H I cloud candidates shows a power law relationship between the sizes and the velocity dispersions of the clouds roughly following the Larson Law scaling $\sigma_v \propto R^{0.5}$, with steeper indices associated with dynamically hot regions. The clouds in each catalog have roughly constant virial parameters as a function mass suggesting that the clouds are all in roughly the same dynamical state, but the values of the virial parameter are significantly larger than unity showing that turbulent motions dominate gravity in these clouds. The mass distribution of the clouds is a power law with differential indices between -1.6 and -2.0 for the three catalogs. In contrast, the distribution of mean surface densities is a log-normal distribution.

Subject headings: galaxies: individual (Large Magellanic Cloud) — galaxies: ISM — ISM: neutral hydrogen — Magellanic Clouds — radio lines: galaxies

¹Department of Astronomy & Space Science, Sejong University, KwangJin-gu, KunJa-dong 98, Seoul, 143-747, Korea; e-mail: sek@sejong.ac.kr

²Harvard-Smithsonian Center for Astrophysics, 60 Garden St., MS-66, Cambridge, MA 02138, USA

³Korea Astronomy and Space Science Institute, Daejeon, 305-348, Korea

⁴Physics Department, Louisiana State University, LA 70803, USA

⁵Mount Stromlo Observatory, Weston Creek, PO Box, ACT 2611, Australia

⁶IBM Research Division, T.J. Watson Research Center, P.O. Box 218, Yorktown Heights, NY 10598, USA

⁷Australia Telescope National Facility, Epping 76, NSW2121, Australia

⁸Astronomy Department, University of Illinois at Urbana-Champaign, West Green St., IL61801, USA

1. Introduction

It is well known that interstellar turbulence is a vital element of theories of star formation. During the last decade, theoretical models of the importance of turbulence on star formation have been produced (Scalo and Elmegreen 2004, for a review) using observations to provide constraints to the models. MacLow and Klessen (2004) stress that the size line width scaling relation can arise from the fact that molecular clouds are hierarchical structures in turbulent flow and theory of turbulence leads to a log-normal probability gas density function (Padoan and Nordlund 2002).

A 21 cm neutral hydrogen interferometric survey of the Large Magellanic Cloud (LMC) (Kim et al. 2003) combined with the Parkes multi-beam H I single-dish survey (Staveley-Smith et al. 2003) clearly shows that the H I gas is distributed in the form of clumps or clouds as well as shells (Kim et al. 1999). These features are also well demonstrated in the ATCA survey alone (Kim et al. 1998). Wada et al. (2000) present that high-resolution 2D numerical simulations of the interstellar atomic hydrogen gas in the LMC and find that the statistical properties of H I from their simulation are similar to those of observed H I from the ATCA interferometry survey.

In this present study, we present catalogs of various clump-like or cloud-like features in the LMC using the combined ATCA+Parkes survey. The LMC is the nearest disk galaxy to the Milky Way but its face-on geometry avoids the complications of the line-of-sight blending that pose difficulties in studying discrete H I clouds in the Milky Way. This paper presents the properties of the H I clouds and compares those properties to the scaling relationships for the atomic and molecular gas in the Milky Way.

2. The Cloud Catalog

This section describes the selection criteria for the H I cloud candidates chosen from the H I data cube of the LMC. The H I clouds were identified using a brightness temperature threshold (T_b) applied to the 21-cm neutral hydrogen gas survey of the LMC. We cataloged the data from the combined surveys (Kim et al. 2003) of the Australia Telescope Compact Array (ATCA) (Kim et al. 1998) and the Parkes 64-m single-dish telescope (Staveley-Smith et al. 2003). The results of H I aperture synthesis mosaic survey were made by combining data from 1344 separate pointing centers and the Parkes 64-m multi-beam data correspond to $11^{\circ}.1 \times 12^{\circ}.4$ on the sky. The spatial resolution of the map is $50'' \sim 55''$ corresponding to a physical resolution of $12 \sim 14$ pc at the distance of the LMC (Alves 2004). The observing band was centered on 1.419 GHz, corresponding to a central heliocentric velocity coverage

from -33 to $+627$ km s $^{-1}$ with a velocity resolution of $\delta v \equiv 1.649$ km s $^{-1}$. Using the technique, a variant of approach described by Schwarz and Wakker (1991), a composite image was formed by filtering out the short spacing data from the ATCA image and then adding the Parkes image. The Fourier transformed Parkes images were added to the final images with no weighting in MIRIAD task IMMERGE. The RMS noise level of the final cube is $\sigma_{rms}=2.5$ K.

We identify clouds using a brightness temperature threshold and identifying all connected pixels above the temperature threshold as belonging to a single cloud (cf. 5; 27; 26). Ideally, one would like to define clouds with a zero threshold intensity. However, low threshold intensities are impractical in view of the noise level in the spectra and more importantly because of the blending of adjacent clouds which often occur in crowded regions. On the other hand, with too high a threshold intensity, regions are severely truncated, and it is impossible to obtain a reliable estimate of the sizes and velocity dispersions, and related parameters (Scoville et al. 1987). Identification of the clouds are conducted within IRAF¹ with the computer algorithm we have written in FORTRAN. In order to make the FORTRAN code available in the environment of IRAF, a Command Language (CL) for IRAF is used to incorporate compiled code into the CL by calling newly added functions within a CL program. We arbitrarily simplify the CL file for easy handling. One merit of making a task within IRAF is that every data can be handled in IRAF image form, which can be transformed to FITS form easily, and can be transported to other reduction packages, if necessary. Moreover, the identified clouds can be separately regenerated for further analysis within IRAF. When making a catalog of identified clouds, one may adjust the threshold pixel numbers, as one may not want to include the minimum number of pixels for defining a cloud. Along with identifying clouds, the algorithm calculates intensity-weighted mean values of longitude, latitude, and velocity as well as these the dispersions of these parameters. In addition, the total integrated intensity, the number of identified clouds, and the number of pixels involved are also reported.

We adopt three separate temperature thresholds: $T_{thresh}=64$, 32, and 16 K, identifying 195, 406, and 468 clouds at each threshold level. A pixel identified as part of a cloud at high thresholds will also be included in catalogs at lower thresholds (cf. Scoville et al. 1987). The catalogs respectively contain 3, 19 and 37 % of the total luminosity in the data cube. We do not apply a minimum size criterion to the clouds included in the catalog, so objects as small as 1 pixel are nominally included though few objects this small are identified (see §3.2).

¹Image Reduction and Analysis Facility is written and supported by the IRAF programming group at the National Optical Astronomy Observatories.

For a cloud consisting of a set of pixels with positions $\{x_i, y_i, v_i\}$ and intensity $\{I_i\}$. The mean velocity for a cloud is calculated as the intensity weighted mean over all the pixels within a cloud:

$$\langle v \rangle = \frac{\sum_i v_i I_i}{\sum_i I_i} \quad (1)$$

where I is intensity of a pixel and i runs over all pixels in the cloud. The velocity dispersion (σ_v) is also intensity-weighted:

$$\sigma_v^2 = \frac{\sum_i I_i (v_i - \langle v \rangle)^2}{\sum_i I_i}. \quad (2)$$

where $\sum_i I_i$ is the integrated intensity of pixels within the cloud.

We have also observed the internal velocity dispersions and sizes of the identified H I clouds. We define the internal velocity dispersion as the rms magnitudes of gas motions along individual lines of sight (at position x, y) with respect to the average cloud velocities along those directions. The observed dispersion of each line of sight, $\sigma(x, y)$, is derived from:

$$\sigma^2(x, y) = \frac{\sum_k I_k [v_k - v_c(x, y)]^2}{\sum_k I_k} \quad (3)$$

where $v_c(x, y)$ is the centroid velocity at position (x, y) and the sum k runs over all pixels in the cloud with position (x, y) . The centroid velocity at this position is:

$$v_c(x, y) = \frac{\sum_k I_k v_k}{\sum_k I_k}. \quad (4)$$

The internal velocity dispersion of the entire cloud is then given by

$$\sigma^2 = \frac{\sum_{ij} [\sigma^2(x_i, y_j)] W_{ij}}{\sum_{ij} W_{ij}}. \quad (5)$$

where the summation \sum_{ij} runs over all x, y positions in the data cube and W_{ij} is the integrated intensity for each position. The internal velocity dispersion is an attempt to remove the effects of the point-to-point velocity differences in the centroid of the cloud (such as velocity gradients in the cloud). Therefore, the total velocity dispersion (Equation 2) is a mixture of the large-scale velocity variations across the region and the smaller-scale motions responsible for the line width, since the thermal contribution is negligible.

The size of each cloud is calculated from based on its extent in the spatial dimension. We measure the second moment of the emission around the centroid of emission:

$$\sigma_x^2 = \frac{\sum_i I_i (x_i - \langle x \rangle)^2}{\sum_i I_i}. \quad (6)$$

with a similar expression for σ_y . The radius (size) of a cloud is then reported as

$$R = (2 \ln 2 \sigma_x \sigma_y)^{1/2} \quad (7)$$

We make no correction to the size for beam convolution effects. Since the radius is calculated from a dispersion, clouds must be at least two pixels across in both directions.

The mass of the cloud is determined by its luminosity in the 21-cm line with no corrections for optical depth effects. For an integrated intensity W measured in K km s⁻¹,

$$M_{\text{cloud}} = 1.822 \times 10^{18} W A_{\text{cl}} m_{\text{H}} \quad (8)$$

where A_{cl} is the total area of the cloud in cm². No correction for the presence of helium or metals is included in the mass measurement. The potential uncertainties in estimating masses of the H I gas clouds include the importance of H I self-absorption correction to the H I column densities and the existence of molecular gas clumps not traced by CO within the apparent diffuse H I gas (Grenier et al. 2005). Given that $N_H/\tau \approx T_s \Delta V$, where N_H is column density, T_s is spin temperature, T_s and τ cannot be independently determined (Dickey and Lockman 1990). Thus, it is not easy to determine a definite N_H in the optically thick case from the line analysis.

The physical parameters of the individual H I cloud candidates are reported for each catalog in Tables 1 through 3. Between the catalog, the H I clouds are similar in structure, but appear to be inhomogeneous and clumpy in nature as seen in Figure 1 and Figure 2. H I clouds often express similar pattern to those of molecular clouds (Heiles 1997). Large clumps within molecular clouds have been observed to contain a number of smaller clumps moving randomly (Myers 1978; Blitz 1980). For decades, observations of molecular clouds have shown that the internal velocity dispersion of each region is well correlated with its size and mass; this is known as the Larson's scaling law (Larson 1981). Observations of non-thermal line widths indicate the turbulent nature of the interstellar clouds (Falgarone and Phillips 1990).

3. Discussion

3.1. Distribution of H I cloud candidates

This study is directed at revealing the cloudy nature of the atomic interstellar medium (ISM) in the LMC. The locations of identified H I cloud candidates are shown in Figure 1. In Figure 1, we plot the location and sizes of H I clouds in the LMC. The LMC is nearly face-on ($i = 22^\circ - 33^\circ$) and the synthesized beam is 50''–55'' in diameter, which

corresponds to a spatial resolution of 12–14 pc in the disk of the LMC at the distance of the LMC (50.1 kpc, Feast 1991; Alves 2004). It is interesting to note smaller clouds identified with a higher brightness temperature threshold inside a big cloud with a lower brightness temperature threshold. This feature might indicate the hierarchical structure of the neutral hydrogen gas in the ISM. We note that the sizes of the H I cloud candidates do not depend on their locations in general. Regardless of the brightness temperature threshold, a total of 87 H I cloud candidates lie close to the northern H I spiral arm and the other 159 H I cloud candidates lie close to the southern H I spiral arm. On the other hand, 823 H I cloud candidates are located in the other regions of the LMC. In contrast to the ^{12}CO emitting clouds in the ^{12}CO $J = 1 \rightarrow 0$ map of the LMC by the NANTEN 4-m telescope (Fukui et al. 2001), the H I cloud candidates identified here in the present study distribute quite uniformly. In general, there is no major concentration of H I cloud candidates in any part of the LMC (Figure 2). We highlight several regions of the LMC in Figure 2 associated with dynamically “hot” regions like 30 Doradus or the supergiant shell LMC 4 (Meaburn 1980) and label associated clouds in Tables 1–3.

For a given temperature threshold, H I cloud candidates both in the dynamically hot regions and in the other regions obey the power law relationship between the size R and the velocity dispersion σ of H I cloud candidates as shown in Figures 4, 5, and 6. These phenomena are similar to the Larson Law in its characterization of molecular clouds. The dynamically hot regions are characterized by quantitative measurements of turbulence. The velocity difference map (Figure 8 in Kim et al. 1998) generated from the modulus of the velocity difference between the peak radial velocity and the velocity smoothed over to an effective resolution of $20'$ can help us to quantify dynamically hot effects in the ISM. The velocity dispersions σ of the H I clouds increase with their sizes L as power law, $\sigma \propto L^\alpha$. A slope α of velocity dispersion to size relation of H I cloud candidate in the dynamically hot regions varies logarithmically from 0.33 ± 0.14 to 0.88 ± 0.32 . A slope of the power law relationship between velocity dispersion and size appears to be similar as $0.46(\pm 0.06)$ – $0.52(\pm 0.04)$ in the relatively quiet regions. Figure 7 presents a slope of the power law between the size and the velocity dispersion in the entire regions of the LMC for a given brightness temperature threshold by which the H I cloud candidates were identified and selected. It is suggested that the slope of size–velocity dispersion relation varies from 0.48 to 0.53, depending on the locations of clouds and the temperature threshold. In regions other than 30 Doradus, the spiral arms, LMC 4, and the western end of bar, the slope does not vary much with the temperature threshold. The arithmetic mean value of slopes seen in Figure 7 is about 0.5 ± 0.02 which seems to match values obtained by other studies in the statistical uncertainties and similar to the Kolmogorov value. Our derived slope in some of dynamically hot regions for a given brightness temperature threshold is significantly higher than exponent of

Larson size-line width relation, 0.38.

In recent studies (Hennebelle et al. 2006; Vázquez-Semadeni et al. 2006), synthetic H I spectra have been computed and the CNM clouds are formed in their numerical simulations. In their simulations, the CNM clouds are formed by dynamical compressions in the WNM, appear to have velocity dispersions of about 1 km s^{-1} , and follow Larson-type relations. They find that the velocity dispersion increases with the size of the CNM structures, L , as $\sigma \propto L^{0.4}$. Their velocity dispersions are comparable to the values observed in H I clouds by Heiles & Troland (2003). In our case, cold and warm gas are mixed. As expected, typical velocity dispersions are 1.5–4 times larger than theirs depending on the threshold used to define the clouds.

3.2. The Mass Spectrum of H I Cloud Candidates

In Figure 7, we plot the cumulative mass distribution of cloud candidates for the three catalogs given in Tables 1 to 3. The cumulative mass distribution plots the number of clouds with a mass greater than a given mass. The cumulative mass distribution is the integral of common differential mass distribution (dN/dM):

$$N(M' > M) = \int_M^\infty \frac{dN}{dM'} dM' \quad (9)$$

We choose the cumulative mass distribution rather than the differential distribution because (1) estimates of the differential mass distribution are prone to systematic errors due to binning choice and (2) fits to the cumulative mass distribution can account for uncertainties in the cloud mass which analyses of the differential mass spectrum commonly neglect (Rosolowsky 2005). For each catalog, we fit a power law function to the cumulative mass distribution.

$$N(M' > M) = N_0 \left(\frac{M}{10^5 M_\odot} \right)^{\gamma+1} \quad (10)$$

N_0 is the number of clouds in the derived distribution with masses larger than $10^5 M_\odot$ and γ is the index of the differential mass distribution. For $\gamma > -2$, the mass distribution is top heavy and most of the mass is found in the high mass clouds. For $\gamma < -2$, the opposite is true; and $\gamma = 2$ implies an equal amount of mass in every logarithmic bin of the mass distribution.

For each mass distribution, we estimate the parameters of the mass distribution using the algorithm of Rosolowsky (2005). The adopted algorithm is a non-linear regression of the data to Equation 10 using the error-in-variables method (3) for parameter estimation.

The uncertainties in the cumulative mass function are given by counting errors and the uncertainties in the mass function are assumed to be 5%. We report the derived parameters for the mass distributions of the three catalogs in Table 4. For each catalog, we adopted a different completeness limit appropriate for that catalog and reported this value in Table 4. Since clouds down to the size of 1 spatial resolution element by 1 velocity channel are included in the catalog, it would appear that the completeness limit is set by our brightness threshold:

$$M_{comp} = 0.014 \ell^2 \delta v T_{thresh} M_\odot \quad (11)$$

where ℓ is the linear extent of 1 pixel in pc and δv is the channel width in km s⁻¹. For a pixel size of 9.7 pc and a channel width of 1.649 km s⁻¹, the completeness limit is 3.7, 7.3 and 14.6 M_\odot for $T_{thresh} = 16, 32$, and 64 K respectively. Inspection of Tables 1 to 3 or Figure 7 shows no clouds with such a low mass are found in the catalog, though they should be detectable. Such clouds are not detected because the ISM of the LMC does not contain clouds with these properties. We find that the clouds in the LMC are all drawn from populations with roughly constant virial parameter (see below) and clouds with such a low mass would have sizes and line widths significantly smaller than the beam width and channel size and thus be undetectable given the data.

The adopted limits are, instead, inferred from extrapolations of the dynamical states (virial masses) of the clouds down to a dynamical completeness limit established by the resolution of the observations. The dynamical mass estimate for a cloud is given by

$$M_{VT} = \frac{5R\sigma_v^2}{\alpha G} \quad (12)$$

where α is the virial parameter for the clouds. If the clouds are self-gravitating and complicating effects such as magnetic fields or external pressure are negligible, $\alpha < 2$. Virialized clouds have $\alpha \approx 1$. In Figure 8, we plot the dynamical mass estimate ($5R\sigma_v^2/G$, i.e. the virial mass with α assumed to be unity) as a function of the total luminous mass (μM_{21cm} , where $\mu = 1.4$ is the mean particle mass accounting for metals and helium). The cloud populations stretch out along loci of constant virial parameter α . We plot the median virial parameter for each catalog as a gray line. For a 64, 32 and 16 K threshold, we find median virial parameters of $\langle \alpha \rangle = 7.2, 13.9$, and 28.2 respectively. The apparent differences in virial parameters for the cloud catalogs are a consequence of changing the threshold contour $\langle \alpha \rangle \propto T_{thresh}^{-1}$ with no attempt to account for emission below the threshold level. Since the mean virial parameters are significantly larger than unity, self-gravity is negligible for these clouds and their internal energetics are dominated by their kinetic energy (See §3.3).

The distribution of dynamical mass estimates is truncated at the dynamical completeness limit given by the horizontal dotted line. This limit is defined as the dynamical mass

limit for $R = 2\ell = 19.4$ pc and $\sigma_v = 0.5R^{0.5} = 2.20$ km s $^{-1}$. Note, we have used the velocity dispersion implied by size-line width relationship (Figure 6) since is this larger than what would be implied by the channel width [$\sigma_v = \delta v/(8 \ln 2)^{1/2} = 0.71$ km s $^{-1}$]. Thus, it is the spatial resolution which defines how deep into the LMC cloud population the catalog samples. Similarly, the luminous mass distribution is truncated at the vertical dotted line established by the threshold temperature and the minimum radius and line width given above. We adopt the completeness limits given in Table 4 so that the completeness limit is above where the lower envelope of the data intersects with the dynamical completeness limit and the left-hand envelope of points is similarly above the intersection with the luminous mass completeness limit. Points found below the dynamical completeness limit have unreliable estimates of their sizes or line widths because these cloud properties are affected by pixelization.

Returning to the mass distributions, we find that a power law distribution is a good model for all but the most massive clouds in each catalog. For the higher thresholds (64 and 32 K), the index of the mass distributions is $\gamma \approx -1.7$, but the distribution significantly steepens to be consistent with $\gamma \approx -2.0$ at lower thresholds. Unlike the mass distributions of GMCs in the LMC (Mizuno et al. 2001; Blitz et al. 2007), there is no evidence for a truncation of the mass spectrum at large masses. Indeed, the opposite seems true: the maximum mass clouds are significantly more massive than predicted by the power-law distribution. All of the “overmassive” clouds are found associated with the star-forming bar in the LMC and this suggesting a difference in the structure of the ISM for this region.

Many turbulent models of the ISM predict a log-normal distribution of object masses (e.g. Ostriker et al. 2001), so we also fit the cumulative value function of a log-normal distribution to the each of the catalog distributions:

$$N(M' > M) = \frac{N_0}{2} \left[1 + \text{erf} \left(\frac{\ln M - \ln M_0}{\sigma_{\ln M}} \right) \right]. \quad (13)$$

The results of the fits are shown in Figure 9. The residuals of the log-normal distribution show significant excursions outside the counting uncertainties, particularly when compared to the residuals of the power law fits indicating that a power-law model of the mass distribution is superior to that of a log-normal distribution for these data.

Wada, Spaans, and Kim (2000) argued that an index of power law fit can be steeper if there is star formation ongoing, so the dissipation of clouds occurs. In the presence of star formation (their SF2 simulation), they argued that the mass spectrum shows roughly $dN/dM \propto M^{-2.3}$ for a brightness temperature threshold of 50 K which is steeper than the comparable index for the 21-cm masses where $T_{\text{threshold}} = 64$ K: $\gamma = -1.68 \pm 0.04$. Wada et al. (2000) also report that $dN/dM \propto M^{-2.7}$ for a brightness temperature threshold of 30 K

and the derived index for $T_{threshold} = 32$ K is $\gamma = -1.65 \pm 0.04$. The resulting catalogs in the LMC have, in general, a shallower mass distribution than the simulations and there is not a significant change in the distribution between the 64 and 32 K thresholds. However, when the threshold is decreased to 16 K, probing the lowest mass clouds, the index $\gamma \approx -2.0$. For an index value $\gamma = 2$ there is equal mass in each logarithmic bin of the mass distribution implying the mass structure of the ISM for low surface brightness clouds have no preferred mass scale.

3.3. The Dynamical State of H I Clouds

In Figure 10 we compare the virial parameter for H I clouds in the the LMC to that of the GMCs. The virial parameter is defined so that the dynamical and luminous mass estimates will be equal. The virial parameter is plotted as a function of the total luminous mass. As seen in Figure 8, there is no trend in virial parameter as a function of cloud mass – all H I clouds are in a similar dynamical state. This is in contrast with the work of Heyer et al. (2001) who find that, for molecular clouds in the outer galaxy, high mass clouds show a roughly constant virial parameters, but low mass clouds follow the locus of pressure equilibrium with their surroundings. That the H I clouds show no significant change in virial parameter as a function of mass stands in contrast with the low-mass molecular “chaff” seen in the outer galaxy. This empirical result should be readily predicted by simulations of the galactic-scale ISM.

The virial parameter also appears to be constant for the GMCs in the LMC, except their virial parameter is significantly lower $\langle \alpha_{GMC} \rangle = 1.8$. The large margin between the virial parameters for the two populations of clouds indicates that even the brightest, most massive components of the LMC highlighted in the $T_{thresh} = 64$ K catalog are not identifying atomic counterparts to GMCs but rather larger turbulent structures in the ISM.

3.4. The Mass-Radius Relationship

Since the H I clouds have roughly constant virial parameters for a given threshold and also follow a size-line width relationship, the clouds should also follow a mass-radius relationship. Such a relationship is plotted in Figure 11. Linear fits to $\log(M)$ as a function of $\log(R)$ give $M \propto R^{2.05 \pm 0.10}$ for all the catalog with the constant being established by the adopted threshold temperatures. The mean surface densities of the clouds $\langle \Sigma \rangle = \langle M/\pi R^2 \rangle$ are 4.7, 2.5 and 1.3 $M_\odot \text{ pc}^{-2}$ for $T_{thresh} = 64, 32$, and 16 K respectively, scaling inversely

with threshold implying that the variation is entirely due to the changing threshold values. Such low column densities stand in contrast with the column densities of molecular clouds in the LMC where $\langle \Sigma_{GMC} \rangle = 50 M_\odot \text{ pc}^{-2}$ (2).

The cumulative size distribution for the identified H I clouds is also shown in Figure 14. We fit power-law distributions to the size distribution. For a power law of the form $dN/dR \propto R^\beta$, we find indices of $\beta = -2.2, -2.3, -3.0$ for the temperature threshold, 64, 32, 16 K, respectively. It is interesting to note that $\beta \approx -3.0$ at the lowest temperature threshold is the steepest and similar to that found for the size spectrum of molecular clouds observed in CO $J = 2 \rightarrow 1$ and CO $J = 1 \rightarrow 0$ (Heithausen et al. 1998; Kramer et al. 1998).

For comparison, cumulative distribution of mean column density distribution of H I gas in the LMC along the line of sight are given in Figure 12 for the individual catalogs and for all positions in the map in 13. Neither the cumulative distribution of H I surface density nor the probability distribution function of observed column density along the line of sight yield a power law fit. Instead, the column density histogram appears to have a log-normal distribution instead and we report the parameters of the log-normal fits in Table 14.

The column density distributions of small CNM structures studied with Arecibo (Heiles and Troland 2005) and extracted from numerical simulation (Hennebelle et al. 2006) follow a power law. Here we also would like to emphasize that the column density spectrum in the present study is not well-reproduced by a power law but rather by a log-normal distribution (in contrast with the mass and radius distributions which are power laws). Two features distinguish our measurement from that of Heiles & Troland (2005): the structures in our catalog are significantly larger than those studied in their work and their observations are based off 21-cm absorption line studies yielding column densities without any assumptions.

3.5. Cloud Aspect Ratios

It is important to note that the present observations also show that the clumped state of H I gas appears embedded in the more diffuse neutral gas clouds. Most clouds are not round, but have an elongated or filament-like shape. The histogram of measured inverse aspect ratio of each H I cloud from the cloud finding algorithm (Figure 15) indicates that the peak distribution of aspect ratio arises between 0.3 and 0.4. The mean inverse aspect ratio is about 0.4 and ranges between 0.38 and 0.42. We note that the mean inverse aspect ratio of the clouds identified with the highest temperature threshold is slightly larger than that of the clouds detected with lower temperature threshold. The presence of smaller and denser H I clump-like objects is likely to be comparable with the cold neutral medium (CNM), one

of the four phases of the interstellar medium (Heiles 2001). As it is now well established, the atomic interstellar medium is thermally bistable as predicted by detailed computations of thermal balance (Field, Goldsmith, and Habing 1969; McKee and Ostriker 1977; Wolfire et al. 1995, 2003). H I gas can be in two different thermodynamical states. A cold neutral medium (CNM) is embedded in a warm neutral medium (WNM) and can coexist in thermal pressure equilibrium (Kulkarni and Heiles 1988). Recently much attention has been paid to the smaller scales of H I emission and its dynamical properties as a result of extensive surveys using interferometers and single-dish telescope (Heiles and Troland 2003). In order to understand the properties of observed H I, numerous numerical simulations have been performed (Dib and Burkert 2005; Gazol, Vázquez-Semadeni, and Kim 2005; de Avillez and Breitschwerdt 2005). Attempting to resolve the warm and cold components in the atomic gas, high-resolution numerical simulations were achieved by various teams (Burkert and Lin 2000; Hennebelle and Péault 2000; Koyama and Inutsuka 2002; Krtsuk and Norman 2002; Piontek and Ostriker 2005; Audit and Hennebelle 2005; Heitsch et al. 2005; Vázquez-Semadeni et al. 2006) and have demonstrated that degree of turbulence in H I gas is crucial to understand phase transformation between the warm diffuse phase and the cold dense phase induced by dynamical condensation.

4. Conclusion

The H I clouds and clumps have been identified and cataloged with a brightness temperature threshold (T_b) from a 21-cm neutral hydrogen gas survey of the LMC, which was created using the combined surveys (Kim et al. 2003) of the Australia Telescope Compact Array (ATCA) (Kim et al. 1998) and the Parkes 64-m single-dish telescope (Staveley-Smith et al. 2003). Using our full data set, observations of H I establish that the Larson size-line width relation is obeyed with exponent similar to the Kolmogorov value (Padoan and Nordlund 2002). The virial parameters of the clouds are all significantly larger than unity implying that turbulent energy dominates the self-gravity of the structures on these size scales. The H I clouds distinct from the GMCs in the LMC which have significantly smaller virial parameters. The mass and size distributions of the clouds are both well-represented by power laws with $dN/dM \propto M^\alpha$ with $\alpha = -1.6 \rightarrow -2.0$ and $dN/dR \propto R^\beta$ with $\beta = -2.5 \rightarrow -3.0$. We find that the clouds have a roughly constant average column density as a function of cloud mass, but that column density is distributed around the mean following a log-normal distribution. Given the simple nature of the observations made, the derived distributions should be easily compared to simulations of the galactic ISM.

We thank A. Goodman and E. Keto for interesting discussion. We thank the anonymous

referee for his/her invaluable comments which have improved the manuscript significantly. SK was supported in part by the Korea Science and Engineering Foundation (KOSEF), under a cooperative agreement with the Astrophysical Research Center of the Structure and Evolution of the Cosmos (ARCSEC). ER’s work is supported by an NSF Astronomy and Astrophysics Postdoctoral Fellowship (AST-0502605).

REFERENCES

- Alves, D.R. 2004, NewAR, 48, 659
- Audit, E., Hennebelle, P. 2005, A&A, 433, 1
- Blitz, L. 1980, gmcq.work, 1
- Blitz, L., Fukui, Y., Kawamura, A., Leroy, A., Mizuno, N., & Rosolowsky, E. 2007, Protostars and Planets V, 81
- Britt, H. & Luecke, R. 1973, Technometrics, 15, 233
- Burkert, A., and Lin,D.N.C. 2000, ApJ, 537, 270
- Kramer, C., Stutzki, J., Rohrig, R., & Corneliusen, U. 1998, A&A, 329, 249
- Dame, T. M., Elmegreen, B. G., Cohen, R. S., & Thaddeus, P. 1986, ApJ, 305, 892
- de Avillez, M., and Breitschwerdt, D. 2005, A&A, 436, 585
- Dib, S., and Burkert, A. 2005, A&A 630, 238
- Dickey, J., and Lockman, F.J. 1990, ARA&A, 28, 215
- Elmegreen, B. G., Scalo, J. 2004, ARA & A, 42, 211
- Falgarone, E., and Phillips, T.G. 1991, IAUS, 147, 119
- Field, G.B., Blackman, E.G., Keto, E. 2006, astro-ph/0601574
- Field, G.B., Goldsmith, D.W., and Habing, H.J. 1969, ApJ, 155, 149
- Fukui,Y., Mizuno,N., Yamaguchi, R., Mizuno, A., Onishi, T. 2001, PASJ, 53, 41
- Gazol, A., Vázquez-Semadeni, and Kim, J. 2005, ApJ, 630, 911
- Goodman, A.A., Barranco, J.A., Wilner, D.J., and Heyer, M.H. 1998, ApJ, 504, 223

- Giovanelli, R., Haynes, M.P., Salzer, J.J., Wegner, G., da Costa, L.N., and Freudling, W. 1994, AJ, 107, 2036
- Gooch,R. 1996, ASPC, 101, 80
- Grenier, I.A., Cassandjian, J.-M., Terrier, R. 2005, Science, 307, 1292
- Heithausen, A., Bensch, F., Stuzki, J., Falgarone, E., and Panis, J.F. 1998, A&A, 331L, 65
- Heitsch, F., Burkert, A., Hartmann, L., Slyz, A., Devriendt, J. 2005, ApJ, 633, 113
- Heiles, C. 1997, ApJ, 481, 193
- Heiles, C. 2001, ASPC, 231, 293
- Hennebelle, P., Péault, M. 2000, A&A, 359, 1124
- Hennebelle, P., Audit, E., Miville-Deschenes, M.-A 2006, astro-ph/0612779
- Heyer, M. H., Carpenter, J. M., & Snell, R. L. 2001, ApJ, 551, 852
- Heiles, C., and Troland, T. 2003, ApJ, 586, 1067
- Heiles, C., and Troland, T. 2005, ApJ, 624, 773
- Heyer, M., & Schloerb, F. 1997, ApJ, 475, 173
- Koyama, H., and Inutsuka, S. 2002, ApJ, 564, L97
- Kim, S., Staveley-Smith, L., Dopita, M. A., Freeman, K.C., Sault, R.J., Kesteven, M.J., & McConnell, D. 1998, ApJ, 503, 674
- Kim, S., Dopita, M.A., Staveley-Smith, L., & Bessell, M. 1999, AJ, 118, 2797
- Kim, S., Staveley-Smith, L., Dopita, M. A., Sault, R. J., Freeman, K. C., Lee, Y., Chu, Y. 2003 ApJS, 148, 473
- Kritsuk, A. G., Norman, M. L. 2002, ApJ, 569, 127
- Kulkarni, S.R., and Heiles, C. 1988, In *Galactic and extragalactic radio astronomy*, 95
- Larson, R. B. 1981, MNRAS, 194, 809
- Lazarian, A. 2004, JKAS, 37, 563
- Mac Low, M.-M., and Klessen, R.S. 2004, Reviews of Modern Physics, 76, 125

- McKee, C.F., and Ostriker, J.P. 1977, ApJ, 218, 148
- Meaburn, J. 1980, MNRAS, 192, 365
- Mizuno,N. et al. 2001, PASJ, 53, 971
- Myers, P. C. 1978, ApJ, 225, 380
- Ostriker, E. C., Stone, J. M., & Gammie, C. F. 2001, ApJ, 546, 980
- Padoan, P., and Nordlund, A. 2002, ApJ, 576, 870
- Piontek, R.A., and Ostriker, E.C. 2005, ApJ, 629, 849
- Rosolowsky, E. 2005, PASP, 117, 1403
- Scalo, J., Elmegreen, B. G. 2004, ARA & A, 42, 275
- Schwarz, U.J., and Wakker, B.P. 1991, IAU Symposium, 131, 188
- Scoville, N.Z., Yun, M.S., Sanders, D.B., Clemens, D.P., and Waller, W.H. 1987, ApJS, 63, 821
- Solomon, P.M., Rivolo, A.R., Barrett, J., & Yahil, A. 1987, ApJ, 319, 730
- Stark,A., Lee,Y. 2005, ApJ, 619, 159
- Staveley-Smith, L., Kim, S., Calabretta, M. R., Haynes, R. F., Kesteven, M. J. 2003, MNRAS, 339, 87
- Vázquez-Semadeni, R.A., Baume,G., Feinstein,A., Prado, P. 1997b, yCat, 41240013
- Vázquez-Semadeni, E., Ryu, D., Passot, T., González, R., Gazol, A. 2006, ApJ, 643, 245
- Wada,K., Spanns,M., Kim,S. 2000, ApJ, 540, 797
- Wolfire, M.G., McKee, C.F., Hollenbach, D., and Tielens, A.G.G.M. 1995, ApJ, 453, 673
- Wolfire, M.G., McKee, C.F., Hollenbach, D., and Tielens, A.G.G.M. 2003, ApJ, 587, 278
- Williams,J.P., Blitz,L., McKee,C.F. 2000, prpl.conf, 97

Table 1. Catalog of H I cloud for the brightness temperature threshold of 16 K

ID	RA (J2000)	DEC (J2000)	SIZE (pc)	Vel (kms ⁻¹)	σ (kms ⁻¹)	M_{cloud} (M_{\odot})	REGION
1	4:30:39.60	-69:05:24.00	51.180	251.71	1.456	9601.75	
2	4:33:11.04	-69:17:60.00	21.948	247.22	1.996	2178.55	
3	4:34:10.32	-69:22:19.20	19.437	253.31	1.242	1452.37	
4	4:34:30.24	-67:16:51.60	14.845	265.00	1.594	1048.93	
5	4:35:16.56	-68:59:38.40	17.142	249.02	1.465	1129.62	
6	4:35:23.28	-67:13:40.80	20.283	258.75	1.926	2178.55	
7	4:35:36.48	-70:52:44.40	15.969	236.28	0.449	645.50	
8	4:35:43.20	-69:09:25.20	21.971	244.99	1.433	1452.37	
9	4:36:09.60	-66:39:43.20	24.565	274.60	2.443	3953.66	
10	4:36:29.52	-67:28:51.60	22.091	266.30	1.402	1452.37	
11	4:36:49.44	-69:06:25.20	24.883	244.32	0.732	887.56	
12	4:36:56.16	-70:34:04.80	40.188	242.88	2.012	4599.16	
13	4:37:09.60	-67:21:36.00	21.513	261.06	1.674	1129.62	
14	4:37:29.52	-68:48:43.20	16.833	254.12	1.363	1452.37	
15	4:37:36.00	-68:42:07.20	20.994	255.27	1.127	1694.43	
16	4:37:42.72	-66:26:45.60	16.988	276.90	1.704	1048.93	
17	4:38:02.64	-66:19:04.80	91.856	272.21	3.739	70036.32	
18	4:38:02.64	-65:38:13.20	20.616	266.89	1.561	2259.24	
19	4:38:09.36	-66:38:38.40	33.666	270.84	2.167	3953.66	
20	4:38:22.80	-65:17:49.20	28.055	279.18	1.361	3550.23	
21	4:39:22.80	-66:47:02.40	22.444	264.86	0.920	1129.62	
22	4:39:22.80	-69:27:07.20	150.350	245.96	3.334	108846.76	
23	4:39:56.16	-68:09:03.60	20.894	271.11	2.058	1936.49	
24	4:40:09.60	-70:28:58.80	33.195	260.20	3.509	5244.65	
25	4:40:36.24	-66:24:14.40	28.167	262.82	2.019	3469.54	Northern Arm
26	4:40:56.40	-65:50:09.60	47.611	272.76	4.754	11941.68	Northern Arm
27	4:41:29.76	-64:39:39.60	17.325	261.18	0.984	726.18	
28	4:41:43.20	-65:46:08.40	29.478	261.79	2.899	8230.07	Northern Arm
29	4:41:43.20	-67:02:20.40	20.994	282.66	1.540	2017.17	Northern Arm
30	4:41:49.92	-70:54:54.00	36.436	236.44	2.898	7019.77	
31	4:42:03.36	-68:56:20.40	21.683	264.99	0.989	887.56	Northern Arm
32	4:42:03.36	-65:34:37.20	20.565	278.77	1.529	2017.17	Northern Arm
33	4:42:30.24	-71:16:04.80	30.733	242.04	1.968	4841.22	
34	4:42:50.40	-68:08:34.80	15.969	255.54	0.889	564.81	Northern Arm
35	4:42:50.40	-65:16:44.40	18.778	270.72	1.463	1694.43	
36	4:42:57.12	-69:27:50.40	70.462	253.34	2.798	41069.68	Northern Arm

Table 1—Continued

ID	RA (J2000)	DEC (J2000)	SIZE (pc)	Vel (km s ⁻¹)	σ (km s ⁻¹)	M_{cloud} (M_\odot)	REGION
37	4:43:10.56	-64:53:49.20	44.430	267.53	2.300	14039.54	
38	4:43:17.28	-65:38:38.40	36.536	276.06	3.009	7826.64	Northern Arm
39	4:43:44.16	-70:22:48.00	50.155	250.09	1.042	5244.65	
40	4:43:44.16	-65:33:32.40	199.305	284.00	4.489	145882.10	Northern Arm
41	4:44:11.04	-71:02:31.20	24.671	229.04	1.491	1613.74	
42	4:44:11.04	-67:55:15.60	52.696	250.48	3.332	10005.19	Northern Arm
43	4:44:31.20	-68:05:27.60	17.655	252.46	1.162	1371.68	Northern Arm
44	4:44:44.64	-71:15:43.20	18.037	248.68	1.364	887.56	
45	4:44:44.64	-65:10:15.60	19.545	287.40	1.662	1775.11	
46	4:44:58.08	-65:13:37.20	19.356	281.61	0.794	726.18	
47	4:45:04.80	-67:48:10.80	28.018	249.52	1.962	4357.10	Northern Arm
48	4:45:24.96	-70:29:09.60	22.998	256.30	2.501	3469.54	
49	4:45:31.68	-67:53:34.80	17.565	251.73	1.375	968.24	Northern Arm
50	4:45:31.68	-66:26:13.20	16.262	284.57	1.492	726.18	Northern Arm
51	4:45:31.68	-67:01:40.80	19.545	296.42	1.190	1613.74	Northern Arm
52	4:45:31.68	-71:07:55.20	21.971	231.66	0.472	806.87	
53	4:45:45.36	-71:06:54.00	62.933	246.13	3.985	14765.72	
54	4:45:52.08	-65:56:02.40	82.159	282.13	4.388	27675.64	Northern Arm
55	4:46:05.52	-71:16:51.60	17.979	246.40	0.490	726.18	
56	4:46:12.24	-71:13:55.20	21.489	250.23	1.672	1290.99	
57	4:46:18.96	-69:49:55.20	38.426	254.15	1.631	6293.59	Northern Arm
58	4:46:18.96	-64:25:26.40	15.536	267.97	1.000	887.56	
59	4:46:32.40	-71:12:25.20	18.889	242.08	3.253	1855.80	
60	4:46:32.40	-71:25:04.80	22.537	241.25	1.536	1936.49	
61	4:46:39.12	-66:01:15.60	16.988	292.83	2.329	2743.36	Northern Arm
62	4:46:46.08	-67:35:06.00	17.325	267.51	0.871	564.81	Northern Arm
63	4:46:46.08	-65:45:10.80	42.238	289.45	2.781	10166.56	Northern Arm
64	4:47:12.96	-65:49:22.80	40.487	273.13	2.439	6777.71	Northern Arm
65	4:47:12.96	-65:41:16.80	15.969	286.39	3.139	1452.37	Northern Arm
66	4:47:26.64	-70:27:18.00	39.397	260.33	1.588	2985.42	
67	4:47:33.36	-71:10:51.60	23.044	238.61	1.853	1855.80	
68	4:48:13.92	-71:24:36.00	59.098	246.56	3.480	11215.49	
69	4:48:20.64	-70:32:16.80	19.356	276.45	1.320	1210.31	
70	4:48:20.64	-65:29:20.40	17.325	282.50	1.828	1775.11	
71	4:49:01.20	-65:17:31.20	15.936	277.80	0.980	726.18	
72	4:49:42.00	-70:36:21.60	21.292	267.59	1.788	2501.30	

Table 1—Continued

ID	RA (J2000)	DEC (J2000)	SIZE (pc)	Vel (kms ⁻¹)	σ (kms ⁻¹)	M_{cloud} (M_{\odot})	REGION
73	4:49:42.00	-71:20:56.40	27.488	235.61	1.970	1775.11	
74	4:50:02.16	-70:30:00.00	29.156	276.29	2.265	4034.35	
75	4:50:36.24	-71:20:24.00	18.553	233.60	1.370	887.56	
76	4:50:49.68	-71:30:46.80	112.472	245.27	4.711	71327.31	
77	4:51:30.48	-71:47:24.00	27.026	257.62	3.180	4357.10	
78	4:51:37.44	-70:16:08.40	20.231	253.43	1.093	1210.31	
79	4:51:37.44	-70:54:43.20	526.857	251.13	5.980	3093458.89	
80	4:52:45.36	-71:55:26.40	60.899	255.03	3.728	48896.32	
81	4:52:59.04	-67:57:21.60	21.948	277.84	1.869	1613.74	Northern Arm
82	4:52:59.04	-66:01:19.20	17.979	279.05	2.567	2339.92	Northern Arm
83	4:52:59.04	-67:50:34.80	16.550	307.48	1.580	1694.43	Northern Arm
84	4:53:05.76	-67:21:50.40	17.325	268.48	1.208	1210.31	Northern Arm
85	4:53:19.44	-70:07:44.40	49.066	249.89	2.263	8310.76	
86	4:53:19.44	-68:01:15.60	18.297	278.00	1.000	887.56	Northern Arm
87	4:53:39.84	-70:00:07.20	25.260	249.93	2.052	4599.16	
88	4:54:13.92	-67:26:27.60	16.294	280.18	0.969	726.18	Northern Arm
89	4:54:20.64	-65:12:03.60	27.697	289.33	3.344	7261.83	
90	4:54:34.32	-72:00:10.80	22.019	255.50	1.735	1936.49	
91	4:54:54.72	-71:49:04.80	34.284	248.98	2.588	4518.47	
92	4:55:08.40	-71:36:39.60	43.703	248.40	1.776	5728.78	
93	4:55:08.40	-66:57:00.00	17.325	268.54	1.123	887.56	Northern Arm
94	4:55:22.08	-68:16:19.20	18.440	296.68	1.715	2017.17	Northern Arm
95	4:55:22.08	-69:52:51.60	62.102	239.65	3.400	23076.48	Northern Arm
96	4:56:03.12	-68:16:12.00	16.833	290.19	1.797	1371.68	
97	4:56:03.12	-65:27:50.40	20.894	292.99	0.850	1129.62	
98	4:56:03.12	-69:32:45.60	18.297	233.20	1.438	1452.37	End of Bar
99	4:56:37.20	-69:17:24.00	16.294	270.90	0.995	806.87	End of Bar
100	4:56:37.20	-71:42:18.00	27.886	242.36	2.586	4115.04	
101	4:57:25.20	-67:25:08.40	18.917	269.52	2.725	2743.36	
102	4:57:25.20	-67:17:09.60	36.879	276.18	3.184	6777.71	
103	4:57:31.92	-70:42:25.20	48.170	267.11	2.219	5809.46	
104	4:57:31.92	-68:06:50.40	73.101	288.65	2.168	18558.01	
105	4:57:31.92	-68:30:39.60	36.565	298.19	2.255	2904.73	End of Bar
106	4:57:38.88	-66:32:24.00	24.458	290.88	2.845	2824.05	
107	4:57:45.60	-71:39:25.20	19.220	251.01	0.953	887.56	
108	4:57:52.56	-70:22:48.00	120.517	246.01	4.929	89078.45	

Table 1—Continued

ID	RA (J2000)	DEC (J2000)	SIZE (pc)	Vel (kms ⁻¹)	σ (kms ⁻¹)	M_{cloud} (M_{\odot})	REGION
109	4:58:19.92	-68:22:37.20	37.848	296.82	4.739	8472.14	
110	4:58:33.60	-71:52:58.80	43.087	248.80	1.877	3469.54	
111	4:58:33.60	-70:05:09.60	21.489	240.82	1.784	3066.11	
112	4:58:40.32	-67:31:33.60	16.645	276.19	0.981	726.18	
113	4:58:40.32	-66:43:01.20	14.342	304.59	1.710	1290.99	
114	4:59:00.96	-67:17:42.00	61.806	263.23	4.848	22430.99	
115	4:59:00.96	-68:16:22.80	22.280	291.00	1.000	887.56	
116	4:59:07.92	-74:34:04.80	52.486	209.78	1.554	4841.22	
117	4:59:21.60	-73:40:04.80	44.134	287.77	1.670	5083.28	
118	4:59:48.96	-70:03:28.80	27.258	261.17	1.550	3630.91	
119	5:00:02.64	-73:47:27.60	49.396	286.28	1.234	3308.17	
120	5:00:09.60	-64:56:06.00	18.778	279.72	2.281	1775.11	
121	5:00:16.32	-70:10:55.20	52.416	243.25	4.989	69229.45	
122	5:00:36.96	-70:05:06.00	30.389	253.35	5.261	7988.01	
123	5:01:04.32	-70:40:12.00	35.443	263.68	2.053	6374.27	
124	5:01:11.28	-68:05:31.20	22.444	295.68	2.541	4518.47	
125	5:01:24.96	-73:28:01.20	25.426	253.50	1.405	1048.93	
126	5:01:24.96	-69:49:19.20	42.263	248.07	2.532	10408.62	End of Bar
127	5:01:31.92	-71:19:55.20	32.508	235.32	2.110	3469.54	
128	5:01:38.64	-68:05:49.20	18.297	275.07	2.517	2501.30	
129	5:01:59.28	-68:18:46.80	20.101	271.05	1.972	2017.17	
130	5:02:06.24	-70:41:20.40	27.142	246.43	1.968	2501.30	
131	5:02:19.92	-69:33:28.80	42.977	256.04	3.141	9359.69	End of Bar
132	5:02:26.88	-70:28:55.20	53.965	256.83	3.729	14281.60	
133	5:02:40.56	-70:06:10.80	21.755	266.12	2.125	3146.79	
134	5:02:40.56	-68:08:13.20	14.195	279.29	3.095	1694.43	
135	5:02:47.52	-71:10:55.20	20.489	254.76	1.385	1694.43	
136	5:02:54.24	-71:01:26.40	22.350	247.51	2.034	1694.43	
137	5:03:01.20	-64:41:09.60	14.084	286.85	1.640	1290.99	
138	5:03:21.84	-73:15:14.40	25.260	261.26	0.967	1210.31	
139	5:03:28.80	-71:14:13.20	35.160	241.69	1.739	4195.72	
140	5:03:35.52	-66:55:58.80	21.755	274.26	1.274	2017.17	
141	5:03:42.48	-68:22:44.40	28.241	284.32	1.476	2743.36	
142	5:03:42.48	-70:15:43.20	22.256	234.50	3.412	2904.73	
143	5:03:56.16	-69:40:55.20	29.424	251.79	1.791	3953.66	End of Bar
144	5:04:03.12	-64:41:13.20	16.926	294.20	0.980	806.87	

Table 1—Continued

ID	RA (J2000)	DEC (J2000)	SIZE (pc)	Vel (kms ⁻¹)	σ (kms ⁻¹)	M_{cloud} (M_{\odot})	REGION
145	5:04:16.80	-73:20:52.80	36.363	252.22	1.625	1694.43	
146	5:04:16.80	-68:52:12.00	50.644	299.39	2.751	12829.23	End of Bar
147	5:04:30.72	-70:42:25.20	111.375	249.77	3.946	76410.59	
148	5:04:37.44	-64:49:01.20	46.710	294.72	2.783	9359.69	
149	5:04:51.36	-74:05:49.20	35.086	293.03	1.259	1775.11	
150	5:04:51.36	-71:30:21.60	17.385	232.09	1.578	1371.68	
151	5:04:58.08	-69:14:52.80	57.496	249.69	2.823	12264.42	End of Bar
152	5:04:58.08	-66:00:-0.00	28.018	280.35	3.127	7181.14	
153	5:04:58.08	-68:32:31.20	17.744	304.17	1.730	1613.74	End of Bar
154	5:05:05.04	-67:02:52.80	55.072	259.60	3.172	17670.45	
155	5:05:12.00	-69:21:36.00	49.903	243.76	1.994	6212.90	End of Bar
156	5:05:18.72	-73:59:31.20	22.537	287.48	0.500	887.56	
157	5:05:25.68	-70:27:50.40	29.424	227.76	1.853	3550.23	
158	5:05:39.36	-65:01:26.40	15.870	291.75	1.619	1210.31	
159	5:05:53.28	-73:56:13.20	37.640	286.70	1.144	2420.61	
160	5:05:53.28	-64:05:20.40	23.203	290.18	1.502	1855.80	
161	5:06:27.60	-68:35:38.40	16.833	225.08	2.371	1210.31	End of Bar
162	5:06:41.52	-67:31:48.00	18.297	232.46	1.795	1613.74	
163	5:06:48.48	-65:43:01.20	25.590	308.88	1.545	1129.62	
164	5:06:55.20	-70:27:50.40	29.317	254.55	2.836	10166.56	
165	5:06:55.20	-68:55:12.00	14.488	288.53	1.174	806.87	End of Bar
166	5:07:02.16	-68:07:19.20	23.044	296.64	0.993	1210.31	
167	5:07:29.76	-66:58:33.60	17.325	278.46	1.599	1371.68	
168	5:07:29.76	-65:34:04.80	22.815	309.02	2.738	2904.73	
169	5:07:43.44	-68:10:04.80	18.610	293.68	1.154	1048.93	
170	5:07:57.36	-65:35:31.20	31.207	286.43	1.686	4599.16	
171	5:08:45.60	-68:15:18.00	16.833	225.81	0.947	726.18	
172	5:08:59.52	-65:11:49.20	23.805	286.21	2.388	2904.73	
173	5:09:06.24	-68:08:09.60	38.590	218.56	3.802	13474.73	
174	5:09:27.12	-69:47:60.00	43.075	254.75	1.710	4115.04	End of Bar
175	5:09:34.08	-69:53:27.60	21.366	240.99	4.514	2339.92	End of Bar
176	5:09:40.80	-73:03:50.40	92.511	255.48	2.519	26142.59	
177	5:09:47.76	-70:56:56.40	33.321	258.67	3.321	5244.65	
178	5:09:47.76	-70:23:31.20	21.948	280.65	1.775	2178.55	
179	5:09:54.72	-65:49:58.80	15.195	296.53	1.093	968.24	
180	5:09:54.72	-68:26:42.00	29.955	311.41	1.717	3308.17	

Table 1—Continued

ID	RA (J2000)	DEC (J2000)	SIZE (pc)	Vel (kms ⁻¹)	σ (kms ⁻¹)	M_{cloud} (M_{\odot})	REGION
181	5:10:01.68	-67:47:13.20	23.937	227.75	2.582	3550.23	
182	5:10:08.40	-64:54:14.40	158.412	295.47	3.058	53818.23	
183	5:10:08.40	-68:19:30.00	35.546	236.02	2.954	9036.94	
184	5:10:22.32	-68:05:34.80	16.391	225.80	2.745	2017.17	
185	5:10:36.24	-70:44:06.00	19.518	237.57	1.780	2017.17	
186	5:10:42.96	-72:54:39.60	17.111	265.22	0.999	726.18	
187	5:10:42.96	-65:59:34.80	22.537	293.72	2.925	3227.48	
188	5:11:17.52	-65:40:37.20	15.056	297.26	0.436	645.50	
189	5:11:24.48	-68:38:06.00	47.611	236.88	2.839	7342.52	End of Bar
190	5:11:31.44	-72:57:14.40	31.988	258.05	1.949	3227.48	
191	5:11:31.44	-66:36:10.80	13.744	281.52	2.387	1210.31	
192	5:11:59.04	-65:43:58.80	20.386	298.52	1.522	1855.80	
193	5:12:19.68	-67:54:39.60	12.336	311.24	2.422	2178.55	
194	5:12:26.64	-68:59:31.20	23.517	216.67	2.660	2097.86	
195	5:12:26.64	-70:11:06.00	15.570	245.06	4.665	2743.36	
196	5:12:33.60	-67:16:58.80	21.415	273.19	1.148	1371.68	
197	5:12:33.60	-67:18:10.80	18.297	300.57	1.875	1694.43	
198	5:12:40.56	-70:06:21.60	28.611	250.47	2.103	4195.72	
199	5:12:40.56	-72:55:08.40	26.378	256.76	2.301	2824.05	
200	5:12:40.56	-64:47:45.60	13.896	293.48	3.500	2259.24	
201	5:13:01.20	-67:02:24.00	26.238	256.67	2.805	4518.47	
202	5:13:01.20	-69:58:04.80	20.944	267.83	3.202	4195.72	
203	5:13:29.04	-69:17:16.80	14.195	208.72	2.986	3550.23	
204	5:13:49.68	-69:16:12.00	20.283	217.00	1.187	968.24	
205	5:14:38.16	-74:14:49.20	21.755	231.82	0.382	806.87	
206	5:14:52.08	-72:59:42.00	49.033	242.40	2.789	8391.45	
207	5:14:58.80	-67:42:36.00	14.845	260.78	2.622	2824.05	
208	5:15:12.72	-66:50:45.60	45.526	282.39	3.665	10166.56	
209	5:15:19.68	-70:02:09.60	15.570	254.81	1.490	1371.68	
210	5:15:33.60	-69:58:01.20	26.318	280.29	3.173	7019.77	
211	5:15:33.60	-74:09:03.60	24.264	235.78	1.612	1290.99	
212	5:15:40.32	-69:56:49.20	17.385	246.78	1.958	1533.05	
213	5:15:40.32	-69:22:37.20	18.917	281.46	1.343	1613.74	
214	5:15:54.24	-72:28:01.20	19.518	262.04	2.072	1694.43	
215	5:15:54.24	-67:39:07.20	22.907	261.48	1.608	1694.43	
216	5:15:54.24	-65:48:10.80	69.154	292.85	2.516	12506.49	

Table 1—Continued

ID	RA (J2000)	DEC (J2000)	SIZE (pc)	Vel (kms ⁻¹)	σ (kms ⁻¹)	M_{cloud} (M_{\odot})	REGION
217	5:15:54.24	-74:05:38.40	25.093	235.71	1.427	1936.49	
218	5:16:15.12	-70:58:30.00	48.061	241.84	2.985	13958.85	
219	5:16:28.80	-64:52:33.60	21.292	297.21	0.844	1533.05	
220	5:17:10.32	-66:28:26.40	43.463	270.98	2.115	6777.71	
221	5:17:10.32	-70:49:04.80	58.041	246.79	1.943	7665.27	
222	5:17:24.24	-69:57:07.20	28.957	219.81	5.182	8149.39	
223	5:17:31.20	-69:48:10.80	65.323	217.09	7.783	50025.94	
224	5:17:52.08	-67:14:31.20	14.739	320.00	1.096	726.18	
225	5:17:58.80	-67:40:44.40	21.586	275.94	2.548	4760.53	
226	5:17:58.80	-70:16:58.80	24.264	229.84	2.583	5486.72	
227	5:17:58.80	-72:47:09.60	18.889	242.27	1.144	968.24	
228	5:18:05.76	-66:15:07.20	26.792	262.59	1.930	3630.91	
229	5:18:19.68	-67:17:38.40	22.537	310.89	1.438	1533.05	
230	5:18:47.52	-72:53:45.60	17.111	249.01	1.773	726.18	
231	5:18:47.52	-70:24:14.40	19.518	282.20	1.530	1290.99	
232	5:18:54.24	-65:31:26.40	42.251	288.54	1.947	4357.10	
233	5:19:22.08	-65:43:51.60	21.755	316.69	1.913	2178.55	
234	5:19:29.04	-72:25:30.00	25.343	254.54	1.248	1371.68	
235	5:19:56.64	-72:41:27.60	126.942	247.33	4.095	78508.45	
236	5:20:10.56	-70:57:10.80	71.269	234.43	3.215	18477.32	
237	5:20:24.48	-72:29:06.00	45.584	257.21	2.495	4599.16	
238	5:20:24.48	-70:14:49.20	17.744	281.96	1.648	1855.80	
239	5:20:38.16	-67:05:42.00	67.340	281.64	2.985	19606.94	
240	5:20:45.12	-70:25:37.20	15.870	238.55	1.348	1129.62	
241	5:21:12.96	-72:48:36.00	42.977	249.77	2.528	4195.72	
242	5:21:12.96	-65:54:32.40	29.263	301.64	3.860	13958.85	
243	5:21:19.92	-67:27:03.60	31.988	271.29	3.362	9521.07	
244	5:21:19.92	-72:16:08.40	18.973	241.55	1.684	1290.99	
245	5:21:26.88	-72:16:08.40	21.292	250.59	2.580	1694.43	
246	5:21:33.60	-67:00:14.40	17.142	278.39	1.977	1452.37	
247	5:21:40.56	-72:29:45.60	32.941	255.94	2.089	3953.66	
248	5:21:47.52	-72:15:36.00	19.518	244.49	0.862	564.81	
249	5:21:47.52	-67:53:52.80	22.067	263.84	4.012	5486.72	
250	5:21:54.48	-72:50:24.00	34.770	249.05	1.788	2017.17	
251	5:21:54.48	-67:48:25.20	14.845	261.04	1.579	1048.93	
252	5:22:01.44	-71:00:50.40	19.811	249.36	1.859	1371.68	Southern Arm

Table 1—Continued

ID	RA (J2000)	DEC (J2000)	SIZE (pc)	Vel (kms ⁻¹)	σ (kms ⁻¹)	M_{cloud} (M_{\odot})	REGION
253	5:22:01.44	-66:23:27.60	16.988	313.39	2.248	2581.98	LMC4
254	5:22:08.40	-66:55:58.80	20.257	275.27	3.231	4115.04	LMC4
255	5:22:08.40	-69:37:12.00	17.385	287.73	2.467	2985.42	
256	5:22:22.32	-67:42:57.60	17.445	281.44	1.358	1371.68	
257	5:22:22.32	-65:08:49.20	22.444	308.85	0.989	1129.62	
258	5:22:29.04	-72:45:07.20	19.598	230.64	2.030	1613.74	
259	5:22:29.04	-66:54:10.80	21.243	290.10	1.641	1855.80	LMC4
260	5:22:36.00	-67:06:25.20	35.487	282.91	2.358	6132.21	LMC4
261	5:22:42.96	-69:28:48.00	24.967	262.05	3.059	3872.98	
262	5:22:42.96	-72:40:58.80	23.717	230.09	1.694	2017.17	
263	5:22:56.88	-66:12:25.20	15.366	316.09	1.600	1371.68	LMC4
264	5:22:56.88	-72:09:43.20	84.687	251.00	3.787	17751.14	
265	5:23:03.84	-65:53:20.40	14.084	289.32	1.766	1290.99	LMC4
266	5:23:10.80	-72:35:06.00	37.388	254.33	1.681	3227.48	
267	5:23:10.80	-67:55:08.40	32.989	238.62	3.914	12667.86	
268	5:23:10.80	-72:07:55.20	19.437	239.50	0.867	564.81	
269	5:23:38.40	-66:01:58.80	16.833	280.87	1.338	1048.93	LMC4
270	5:23:52.32	-72:15:00.00	27.697	254.77	1.843	2904.73	
271	5:23:59.28	-70:07:12.00	64.588	255.19	5.656	26707.40	
272	5:23:59.28	-72:25:40.80	18.610	251.51	0.500	564.81	
273	5:24:33.84	-68:58:40.80	2865.134	274.01	24.386	173786968.77	
274	5:24:47.76	-71:28:12.00	16.988	259.05	0.973	887.56	Southern Arm
275	5:25:15.36	-66:48:36.00	26.378	334.38	4.150	7181.14	LMC4
276	5:25:22.32	-66:54:07.20	19.838	337.10	1.685	2259.24	LMC4
277	5:25:29.28	-69:25:44.40	18.917	272.13	2.082	3388.85	
278	5:25:36.24	-72:46:15.60	20.692	239.64	1.832	1290.99	
279	5:26:04.08	-67:37:26.40	16.645	272.47	2.105	1533.05	LMC4
280	5:26:04.08	-70:00:32.40	26.536	282.48	2.878	4599.16	
281	5:26:24.72	-70:14:16.80	33.416	274.08	3.193	6858.40	
282	5:26:38.64	-66:41:09.60	20.101	284.63	1.999	2501.30	LMC4
283	5:26:38.64	-72:19:40.80	69.668	241.32	3.625	23641.29	
284	5:26:45.60	-66:52:12.00	22.162	304.03	2.091	3953.66	LMC4
285	5:27:06.24	-66:47:52.80	36.822	292.57	3.502	14120.23	LMC4
286	5:27:06.24	-65:27:50.40	31.938	312.54	3.968	4357.10	
287	5:27:20.16	-68:39:10.80	28.018	261.62	1.880	2581.98	
288	5:27:41.04	-66:39:50.40	28.055	289.27	1.910	2501.30	LMC4

Table 1—Continued

ID	RA (J2000)	DEC (J2000)	SIZE (pc)	Vel (kms ⁻¹)	σ (kms ⁻¹)	M_{cloud} (M_{\odot})	REGION
289	5:28:01.68	-66:22:01.20	16.833	292.17	0.955	1048.93	LMC4
290	5:28:01.68	-66:29:24.00	25.590	299.34	1.963	3227.48	LMC4
291	5:28:08.64	-69:35:09.60	22.280	276.78	2.286	3146.79	
292	5:28:08.64	-69:21:18.00	32.718	281.69	2.711	8149.39	
293	5:28:15.60	-72:17:45.60	40.810	251.84	1.846	3308.17	
294	5:28:22.56	-70:26:02.40	14.415	255.81	2.246	1533.05	
295	5:28:50.16	-69:35:38.40	17.385	254.14	1.827	1694.43	
296	5:28:50.16	-65:34:26.40	21.755	324.86	0.881	887.56	
297	5:29:11.04	-69:37:26.40	17.445	250.66	2.294	1613.74	
298	5:29:24.96	-66:16:15.60	21.731	280.28	1.589	2420.61	LMC4
299	5:29:31.92	-70:05:34.80	18.297	251.26	2.411	2178.55	
300	5:29:38.64	-69:40:58.80	29.478	251.03	2.365	2985.42	
301	5:29:38.64	-69:42:10.80	35.041	276.44	3.679	6374.27	
302	5:29:45.60	-69:32:31.20	27.603	254.04	2.662	5083.28	
303	5:30:13.44	-67:25:55.20	30.458	266.06	2.553	3872.98	LMC4
304	5:30:13.44	-72:22:51.60	24.221	238.40	2.711	3146.79	
305	5:30:20.40	-71:11:42.00	21.537	221.04	2.222	2339.92	Southern Arm
306	5:30:41.04	-72:02:06.00	28.611	255.25	1.657	1371.68	
307	5:30:41.04	-69:40:12.00	48.528	243.03	7.608	14039.54	
308	5:30:41.04	-72:30:28.80	104.411	251.22	4.720	44942.66	
309	5:30:48.00	-69:32:56.40	28.975	258.06	5.008	8794.88	
310	5:30:54.96	-70:01:44.40	16.294	257.91	2.096	1210.31	
311	5:30:54.96	-72:35:09.60	28.939	237.69	2.940	3469.54	
312	5:31:08.88	-70:53:06.00	54.613	259.90	2.714	10005.19	
313	5:31:08.88	-68:51:57.60	21.218	273.50	1.786	1855.80	
314	5:31:22.56	-70:55:26.40	17.142	254.51	0.500	564.81	
315	5:31:29.52	-72:33:18.00	20.489	259.70	2.838	2017.17	
316	5:31:43.44	-70:33:54.00	15.870	253.50	2.638	2178.55	
317	5:31:57.12	-72:22:33.60	17.325	254.16	1.622	1048.93	
318	5:31:57.12	-70:48:10.80	13.744	238.70	2.076	1694.43	
319	5:32:04.08	-72:28:26.40	24.069	260.36	2.550	2097.86	
320	5:32:18.00	-67:18:10.80	33.037	295.58	1.745	3469.54	LMC4
321	5:32:24.96	-72:22:30.00	20.386	240.22	0.977	726.18	
322	5:32:38.64	-71:21:57.60	30.613	221.10	2.331	2985.42	Southern Arm
323	5:32:38.64	-72:54:18.00	17.625	272.77	1.560	968.24	
324	5:32:45.60	-72:16:30.00	74.326	253.73	4.417	20171.75	

Table 1—Continued

ID	RA (J2000)	DEC (J2000)	SIZE (pc)	Vel (kms ⁻¹)	σ (kms ⁻¹)	M_{cloud} (M_{\odot})	REGION
325	5:32:52.56	-66:12:25.20	22.677	288.04	2.155	4437.78	LMC4
326	5:32:52.56	-68:35:13.20	32.941	297.39	3.629	5002.59	
327	5:32:59.52	-72:50:06.00	18.889	268.16	1.703	1048.93	
328	5:33:20.16	-65:39:00.00	34.981	318.44	1.905	5809.46	
329	5:33:54.96	-73:05:52.80	51.160	258.02	2.452	6051.52	
330	5:34:08.64	-68:36:07.20	35.590	296.74	2.941	7181.14	30 Dor
331	5:34:08.64	-68:43:22.80	30.903	329.72	2.431	3953.66	30 Dor
332	5:34:15.60	-72:52:48.00	35.957	256.45	3.001	5002.59	
333	5:34:50.16	-67:18:07.20	35.487	265.97	1.832	3711.60	LMC4
334	5:34:50.16	-71:05:24.00	17.979	237.60	1.190	726.18	Southern Arm
335	5:35:17.76	-72:50:49.20	19.437	252.10	1.142	1129.62	
336	5:35:17.76	-69:22:15.60	18.778	258.73	3.556	2501.30	30 Dor
337	5:35:17.76	-65:42:03.60	13.159	312.49	2.243	1775.11	
338	5:35:24.72	-74:40:33.60	19.811	259.64	0.481	806.87	
339	5:35:38.64	-74:45:10.80	66.073	263.36	2.535	12345.11	
340	5:35:45.36	-72:16:26.40	19.518	243.50	0.866	564.81	
341	5:35:52.32	-67:15:18.00	44.181	310.12	3.207	14039.54	LMC4
342	5:35:59.28	-66:29:56.40	40.977	279.50	2.335	7423.20	LMC4
343	5:35:59.28	-67:09:46.80	35.130	300.11	2.846	6777.71	LMC4
344	5:36:19.92	-70:47:42.00	14.195	286.51	1.875	806.87	Southern Arm
345	5:36:33.84	-67:17:31.20	30.613	326.21	3.920	4034.35	LMC4
346	5:36:40.80	-73:02:52.80	35.487	275.93	2.506	3550.23	
347	5:36:40.80	-65:45:18.00	24.778	278.03	1.570	2339.92	
348	5:36:47.76	-72:00:10.80	18.440	229.39	1.476	726.18	
349	5:37:01.44	-65:51:57.60	20.616	272.30	1.937	1936.49	LMC4
350	5:37:01.44	-65:59:20.40	14.009	327.74	1.669	1290.99	LMC4
351	5:37:08.40	-72:53:52.80	57.660	271.01	1.867	8633.51	
352	5:37:15.36	-68:23:02.40	17.655	265.58	1.789	1936.49	
353	5:37:29.04	-71:57:36.00	20.386	257.35	1.376	806.87	Southern Arm
354	5:37:36.00	-68:18:03.60	15.936	270.77	1.195	1048.93	
355	5:37:42.96	-66:47:06.00	20.944	263.92	2.618	3469.54	LMC4
356	5:37:42.96	-71:52:12.00	17.445	229.51	0.874	564.81	Southern Arm
357	5:37:49.92	-67:18:54.00	17.111	330.52	2.482	2420.61	LMC4
358	5:38:03.60	-74:22:22.80	17.744	267.00	1.611	887.56	
359	5:38:10.56	-72:16:55.20	18.440	275.64	1.202	726.18	
360	5:38:17.52	-66:33:57.60	16.988	273.09	2.611	1855.80	LMC4

Table 1—Continued

ID	RA (J2000)	DEC (J2000)	SIZE (pc)	Vel (kms ⁻¹)	σ (kms ⁻¹)	M_{cloud} (M_{\odot})	REGION
361	5:38:17.52	-71:25:15.60	14.488	278.80	2.041	1048.93	Southern Arm
362	5:38:24.24	-74:45:07.20	19.811	275.49	0.858	645.50	
363	5:38:31.20	-68:10:26.40	14.845	270.04	2.012	1210.31	
364	5:38:31.20	-68:49:12.00	33.290	322.53	2.691	4841.22	30 Dor
365	5:38:58.80	-74:48:28.80	25.652	257.73	1.299	1452.37	
366	5:38:58.80	-65:31:19.20	35.767	307.94	2.170	6616.33	
367	5:39:05.76	-66:27:28.80	23.628	280.27	2.838	4357.10	LMC4
368	5:39:26.40	-65:43:30.00	43.463	311.54	1.143	5244.65	
369	5:39:33.36	-68:08:09.60	15.870	272.09	1.858	1048.93	
370	5:39:33.36	-68:35:31.20	19.220	298.35	1.253	887.56	30 Dor
371	5:39:40.32	-66:41:20.40	46.552	270.02	3.035	21946.86	LMC4
372	5:39:47.04	-72:31:48.00	28.223	270.55	1.063	1290.99	
373	5:39:47.04	-65:35:52.80	25.997	306.45	1.520	1694.43	
374	5:40:00.96	-69:17:38.40	54.140	319.54	2.516	16782.90	30 Dor
375	5:40:07.68	-72:26:20.40	12.998	272.07	2.777	1129.62	
376	5:40:14.64	-72:20:24.00	22.998	279.60	0.489	726.18	
377	5:40:14.64	-66:52:44.40	19.758	321.03	2.339	3953.66	
378	5:41:58.08	-68:11:20.40	52.486	278.28	8.533	49864.57	
379	5:41:58.08	-67:22:33.60	12.795	327.34	3.889	1613.74	
380	5:42:05.04	-66:57:21.60	41.486	319.34	3.117	17509.08	
381	5:42:25.68	-71:45:10.80	16.550	267.35	1.511	726.18	
382	5:42:25.68	-65:55:33.60	19.220	314.17	1.409	2420.61	
383	5:42:32.40	-69:20:09.60	18.917	325.82	1.560	1210.31	30 Dor
384	5:42:39.36	-67:58:48.00	23.203	291.10	1.541	1210.31	
385	5:43:06.96	-68:01:37.20	19.705	289.74	2.247	1775.11	
386	5:43:27.60	-67:19:19.20	22.162	315.74	2.318	2743.36	
387	5:43:34.32	-70:38:24.00	38.014	301.73	3.464	4518.47	Southern Arm
388	5:43:34.32	-71:04:44.40	21.342	310.72	1.659	1452.37	Southern Arm
389	5:43:41.28	-66:52:48.00	15.366	290.48	3.240	1936.49	
390	5:43:41.28	-69:12:57.60	17.142	311.50	0.865	564.81	30 Dor
391	5:44:01.92	-71:56:24.00	18.325	278.00	1.000	564.81	
392	5:44:08.88	-70:40:33.60	17.744	297.24	0.426	564.81	Southern Arm
393	5:44:08.88	-67:36:03.60	20.231	316.86	2.701	3308.17	
394	5:44:29.28	-67:10:48.00	15.870	292.97	1.793	1694.43	
395	5:44:29.28	-67:34:40.80	13.278	325.34	1.469	806.87	
396	5:44:49.92	-70:37:12.00	18.440	259.18	1.659	1613.74	Southern Arm

Table 1—Continued

ID	RA (J2000)	DEC (J2000)	SIZE (pc)	Vel (kms ⁻¹)	σ (kms ⁻¹)	M_{cloud} (M_{\odot})	REGION
397	5:45:03.84	-71:54:07.20	21.537	243.15	0.988	968.24	
398	5:45:10.56	-71:40:22.80	24.988	230.29	2.140	1533.05	
399	5:45:17.52	-65:45:10.80	17.655	305.88	1.507	1210.31	
400	5:45:38.16	-73:03:14.40	18.945	280.80	0.980	726.18	
401	5:45:38.16	-65:46:12.00	15.870	302.52	0.500	564.81	
402	5:45:51.84	-67:22:12.00	34.391	284.63	2.419	4437.78	
403	5:45:51.84	-70:33:07.20	18.182	283.43	1.697	1290.99	Southern Arm
404	5:45:58.80	-71:27:28.80	45.075	301.03	2.975	5002.59	Southern Arm
405	5:46:05.52	-71:39:21.60	18.325	301.69	1.168	1048.93	
406	5:46:05.52	-69:38:52.80	22.677	314.20	1.402	1290.99	Southern Arm
407	5:46:26.16	-70:20:13.20	17.744	266.65	1.390	887.56	Southern Arm
408	5:46:32.88	-71:41:31.20	26.078	297.27	1.027	968.24	
409	5:46:53.52	-73:00:18.00	18.917	283.21	0.981	726.18	
410	5:47:07.20	-72:54:54.00	19.811	282.01	0.894	1048.93	
411	5:47:27.84	-70:33:28.80	19.518	284.28	1.695	1613.74	Southern Arm
412	5:48:02.16	-72:52:40.80	17.920	279.52	0.500	564.81	
413	5:48:08.88	-69:52:08.40	18.297	277.37	3.228	1694.43	
414	5:48:08.88	-71:10:12.00	31.072	301.01	2.660	3308.17	
415	5:48:08.88	-69:28:37.20	21.342	319.60	0.801	726.18	
416	5:48:15.84	-72:28:48.00	26.318	286.27	1.196	1694.43	
417	5:48:15.84	-68:24:14.40	21.755	325.70	2.531	2339.92	
418	5:48:36.48	-71:09:21.60	18.037	306.51	0.862	564.81	
419	5:48:50.16	-72:36:14.40	91.799	279.04	2.934	32597.55	
420	5:48:50.16	-70:16:26.40	21.292	288.67	0.944	806.87	
421	5:48:50.16	-70:18:50.40	20.283	309.35	1.495	1129.62	
422	5:48:56.88	-69:02:06.00	15.332	338.00	1.624	887.56	
423	5:49:03.84	-70:12:07.20	15.969	300.01	1.780	726.18	
424	5:49:03.84	-70:55:19.20	20.153	312.61	0.489	726.18	
425	5:49:10.56	-70:40:15.60	44.630	317.26	2.877	5163.97	
426	5:49:17.52	-72:39:32.40	40.188	285.09	1.993	3711.60	
427	5:49:24.24	-71:39:25.20	16.988	298.48	1.124	887.56	
428	5:49:44.88	-70:12:54.00	40.201	315.44	2.557	5083.28	
429	5:49:44.88	-69:14:52.80	26.138	331.13	1.376	1775.11	
430	5:49:58.56	-69:23:49.20	15.091	280.04	1.701	1129.62	
431	5:49:58.56	-66:10:22.80	30.112	287.31	2.493	5406.03	
432	5:50:05.28	-72:43:51.60	28.092	276.17	2.001	2501.30	

Table 1—Continued

ID	RA (J2000)	DEC (J2000)	SIZE (pc)	Vel (kms ⁻¹)	σ (kms ⁻¹)	M_{cloud} (M_{\odot})	REGION
433	5:50:05.28	-67:38:24.00	49.650	285.72	2.770	32113.43	
434	5:50:05.28	-69:48:32.40	19.437	296.36	1.548	1290.99	
435	5:50:12.24	-69:59:56.40	20.075	307.96	2.162	1371.68	
436	5:50:18.96	-70:01:40.80	26.457	303.93	1.438	1452.37	
437	5:50:25.92	-67:09:18.00	20.994	305.00	1.764	1210.31	
438	5:50:39.60	-69:58:26.40	20.944	317.13	1.854	1936.49	
439	5:50:53.28	-69:49:15.60	18.325	266.98	2.138	1694.43	
440	5:50:60.00	-70:03:39.60	17.385	295.45	1.492	726.18	
441	5:50:60.00	-70:05:27.60	35.116	318.94	2.063	5809.46	
442	5:51:06.96	-70:12:00.00	22.444	288.36	2.425	2259.24	
443	5:51:06.96	-70:03:36.00	24.458	307.13	2.027	2097.86	
444	5:51:54.72	-70:16:19.20	27.181	295.51	1.577	2420.61	
445	5:52:35.52	-66:49:08.40	35.723	296.54	2.785	9198.32	
446	5:52:42.48	-70:16:58.80	41.334	304.00	1.806	4437.78	
447	5:52:42.48	-69:51:36.00	24.586	304.50	0.867	1129.62	
448	5:52:49.20	-67:28:22.80	31.741	278.61	1.213	2178.55	
449	5:52:49.20	-67:23:27.60	19.437	286.31	1.700	2017.17	
450	5:52:49.20	-70:27:43.20	23.135	305.00	1.148	806.87	
451	5:52:49.20	-70:09:39.60	31.458	308.43	1.784	3630.91	
452	5:52:56.16	-67:47:52.80	14.195	280.57	1.187	806.87	
453	5:52:56.16	-68:23:24.00	19.437	336.41	1.113	1533.05	
454	5:53:02.88	-70:26:24.00	24.393	299.54	1.260	1371.68	
455	5:53:02.88	-70:22:08.40	22.350	301.45	1.067	1371.68	
456	5:53:16.56	-70:06:18.00	18.325	303.57	2.066	1048.93	
457	5:53:23.28	-66:52:48.00	30.286	293.53	2.049	2824.05	
458	5:53:23.28	-68:42:32.40	16.988	322.46	0.886	564.81	
459	5:53:30.24	-70:11:34.80	18.610	305.27	1.370	887.56	
460	5:53:57.36	-69:04:01.20	17.979	298.01	1.582	1048.93	
461	5:54:04.08	-67:42:03.60	22.792	276.07	1.380	2420.61	
462	5:54:38.16	-69:54:28.80	60.302	289.39	2.902	16056.71	
463	5:54:45.12	-69:43:30.00	24.242	301.95	0.984	1613.74	
464	5:56:13.44	-69:43:33.60	40.926	297.02	1.809	5809.46	
465	5:56:20.16	-67:00:43.20	17.979	293.20	0.988	726.18	
466	6:03:12.48	-69:19:04.80	23.517	274.48	1.143	1694.43	
467	6:03:59.52	-69:16:26.40	16.988	271.49	0.869	564.81	
468	6:07:00.48	-69:42:39.60	17.385	268.79	0.979	726.18	

Table 2. Catalog of H I cloud for the brightness temperature threshold of 32 K

ID	RA (J2000)	DEC (J2000)	SIZE (pc)	Vel (kms ⁻¹)	σ (kms ⁻¹)	M_{cloud} (M_{\odot})	REGION
1	4:37:49.44	-66:18:46.80	33.682	272.59	1.959	8230.07	
2	4:38:36.00	-67:05:60.00	41.914	265.07	4.509	13232.67	
3	4:38:56.16	-66:58:19.20	43.366	261.68	1.612	7988.01	
4	4:39:02.64	-69:27:21.60	37.388	245.36	1.578	5406.03	
5	4:39:36.00	-67:12:54.00	37.834	267.78	1.710	9601.75	
6	4:39:49.44	-67:35:31.20	17.325	267.51	0.871	1129.62	
7	4:40:02.88	-67:45:39.60	55.148	266.07	1.490	15249.84	Northern Arm
8	4:40:09.60	-67:19:44.40	35.957	264.77	1.173	8714.20	Northern Arm
9	4:40:16.32	-67:04:58.80	21.537	267.71	1.943	2743.36	Northern Arm
10	4:40:56.40	-67:28:44.40	21.366	264.99	0.853	2259.24	Northern Arm
11	4:41:09.84	-66:35:31.20	54.478	270.97	1.486	13394.04	Northern Arm
12	4:41:29.76	-67:06:25.20	22.350	262.75	1.384	2259.24	Northern Arm
13	4:41:56.64	-67:45:25.20	22.019	269.24	1.311	3308.17	Northern Arm
14	4:42:30.24	-68:11:20.40	218.414	264.48	6.274	156210.03	Northern Arm
15	4:42:57.12	-70:37:48.00	27.488	248.58	1.629	3953.66	
16	4:42:57.12	-69:28:26.40	55.034	253.01	1.867	14281.60	Northern Arm
17	4:43:03.84	-66:30:18.00	32.909	284.98	1.996	7826.64	Northern Arm
18	4:43:50.88	-67:15:57.60	215.677	272.04	4.299	710045.60	Northern Arm
19	4:43:57.60	-68:36:50.40	27.773	269.98	2.312	3792.29	Northern Arm
20	4:44:37.92	-69:16:04.80	27.373	264.39	2.047	7584.58	Northern Arm
21	4:44:58.08	-65:31:51.60	30.750	284.22	1.481	6051.52	Northern Arm
22	4:44:58.08	-70:45:07.20	175.150	251.96	2.669	141444.31	
23	4:45:11.52	-66:32:42.00	18.383	284.99	2.143	3872.98	Northern Arm
24	4:45:11.52	-68:35:38.40	20.489	267.04	1.849	3550.23	Northern Arm
25	4:45:38.40	-68:02:52.80	23.316	269.00	1.719	3388.85	Northern Arm
26	4:45:45.36	-68:26:20.40	16.833	274.26	0.436	1129.62	Northern Arm
27	4:46:39.12	-68:29:06.00	27.526	280.73	1.711	4034.35	Northern Arm
28	4:46:39.12	-69:30:46.80	18.917	252.25	1.079	2339.92	Northern Arm
29	4:46:39.12	-68:56:02.40	27.200	271.84	1.885	4760.53	Northern Arm
30	4:47:19.68	-67:47:56.40	48.409	272.25	2.211	15007.78	Northern Arm
31	4:48:07.20	-67:01:12.00	222.795	290.54	5.100	1211999.43	Northern Arm
32	4:48:13.92	-67:48:50.40	23.316	279.50	1.454	3872.98	Northern Arm
33	4:48:20.64	-68:43:30.00	34.891	252.81	1.974	10247.25	Northern Arm
34	4:48:34.08	-70:22:48.00	19.437	256.32	0.948	1694.43	
35	4:48:41.04	-70:45:14.40	112.482	253.53	3.918	123451.11	
36	4:49:01.20	-66:35:27.60	16.988	295.22	1.889	3146.79	Northern Arm

Table 2—Continued

ID	RA (J2000)	DEC (J2000)	SIZE (pc)	Vel (kms ⁻¹)	σ (kms ⁻¹)	M_{cloud} (M_{\odot})	REGION
37	4:49:55.44	-70:22:04.80	91.890	254.45	2.739	53818.23	
38	4:50:09.12	-71:30:18.00	19.220	243.03	1.597	1936.49	
39	4:50:42.96	-67:08:38.40	17.979	286.06	1.528	2985.42	Northern Arm
40	4:50:49.68	-70:41:27.60	20.386	250.68	1.235	1775.11	
41	4:50:56.64	-68:54:54.00	690.867	264.20	10.632	8184405.16	Northern Arm
42	4:51:03.36	-68:42:50.40	17.979	260.52	1.121	1775.11	Northern Arm
43	4:52:04.56	-66:15:25.20	17.625	305.41	3.624	7503.89	Northern Arm
44	4:52:04.56	-70:24:18.00	35.428	254.81	1.866	10731.37	
45	4:52:11.28	-69:42:43.20	73.759	244.63	3.456	74877.54	Northern Arm
46	4:52:11.28	-66:51:25.20	30.937	278.46	2.112	13151.98	Northern Arm
47	4:52:52.08	-71:55:30.00	47.335	254.88	1.957	12345.11	
48	4:52:52.08	-67:13:37.20	130.673	291.75	4.727	184531.17	Northern Arm
49	4:53:05.76	-67:37:12.00	25.590	289.84	2.133	8310.76	Northern Arm
50	4:53:19.44	-71:15:43.20	41.461	244.70	2.311	11941.68	
51	4:53:19.44	-70:54:43.20	317.059	252.26	4.598	587401.36	
52	4:53:53.52	-69:48:46.80	22.280	249.37	1.638	2743.36	Northern Arm
53	4:54:00.24	-69:47:42.00	17.385	238.23	1.734	3066.11	Northern Arm
54	4:54:27.60	-69:40:44.40	69.811	269.56	3.347	42683.42	Northern Arm
55	4:54:34.32	-71:18:21.60	30.681	246.91	2.365	6616.33	
56	4:54:34.32	-67:46:58.80	95.854	287.69	7.052	113203.86	Northern Arm
57	4:54:54.72	-65:56:45.60	23.937	294.40	1.552	3953.66	Northern Arm
58	4:55:01.68	-67:00:-0.00	41.789	295.86	2.500	16379.46	Northern Arm
59	4:55:15.36	-70:37:58.80	33.853	265.29	1.999	10892.75	
60	4:55:15.36	-66:05:45.60	620.460	292.41	6.759	5848435.82	Northern Arm
61	4:55:22.08	-65:50:20.40	98.377	306.85	3.157	18396.64	Northern Arm
62	4:55:22.08	-69:23:13.20	24.134	241.49	1.487	3711.60	Northern Arm
63	4:55:35.76	-67:34:51.60	18.297	278.20	0.981	1371.68	Northern Arm
64	4:55:35.76	-69:14:52.80	18.917	257.84	0.987	1452.37	Northern Arm
65	4:55:42.72	-69:55:30.00	77.829	270.84	1.743	19687.63	Northern Arm
66	4:55:49.44	-68:35:31.20	18.610	277.01	1.404	2420.61	Northern Arm
67	4:55:56.16	-71:11:24.00	18.037	249.97	1.000	1129.62	
68	4:55:56.16	-69:30:54.00	16.518	263.73	2.820	4034.35	Northern Arm
69	4:56:09.84	-67:32:13.20	29.797	289.04	2.673	5002.59	
70	4:56:09.84	-67:08:52.80	28.647	290.66	2.170	3872.98	
71	4:56:09.84	-66:39:54.00	16.833	291.34	2.355	2662.67	
72	4:56:09.84	-65:17:60.00	16.067	295.51	2.174	4276.41	

Table 2—Continued

ID	RA (J2000)	DEC (J2000)	SIZE (pc)	Vel (kms ⁻¹)	σ (kms ⁻¹)	M_{cloud} (M_{\odot})	REGION
73	4:56:09.84	-71:19:55.20	28.223	246.95	0.972	4034.35	
74	4:57:18.24	-70:15:14.40	31.408	248.71	1.788	10812.06	
75	4:57:45.60	-71:06:32.40	17.111	248.51	1.695	2743.36	
76	4:57:45.60	-67:38:16.80	33.243	280.53	2.737	14120.23	
77	4:57:52.56	-65:37:26.40	22.091	301.78	1.488	3388.85	
78	4:57:59.28	-66:07:55.20	16.198	282.49	1.345	2259.24	
79	4:57:59.28	-67:01:37.20	72.474	290.14	2.751	59062.88	
80	4:57:59.28	-70:27:03.60	31.741	242.62	2.813	13313.35	
81	4:58:19.92	-71:36:07.20	62.933	241.41	3.403	23560.60	
82	4:58:19.92	-69:26:24.00	111.752	251.65	2.233	65759.90	End of Bar
83	4:58:26.64	-68:09:18.00	16.645	288.81	0.982	1371.68	
84	4:58:33.60	-71:06:57.60	134.164	245.97	2.687	59869.75	
85	4:58:47.28	-70:23:20.40	31.039	249.12	2.644	12506.49	
86	4:58:54.24	-68:40:40.80	29.797	274.25	1.464	8391.45	End of Bar
87	4:59:35.28	-68:38:38.40	17.744	271.72	1.378	1936.49	End of Bar
88	4:59:42.00	-68:06:28.80	111.817	262.07	6.319	124742.10	
89	4:59:48.96	-68:21:10.80	370.816	268.89	5.850	607169.68	
90	4:59:48.96	-69:28:30.00	42.585	251.04	1.847	15249.84	End of Bar
91	4:59:55.92	-67:51:21.60	91.890	257.00	4.345	69390.82	
92	5:00:02.64	-69:35:16.80	15.804	249.20	1.895	2985.42	End of Bar
93	5:00:09.60	-71:42:28.80	19.165	241.19	2.566	2581.98	
94	5:00:16.32	-70:10:55.20	39.517	242.30	3.497	40827.62	
95	5:00:16.32	-66:00:14.40	15.870	297.48	2.734	3792.29	
96	5:00:23.28	-67:02:02.40	21.683	298.29	1.887	5890.15	
97	5:00:36.96	-66:10:58.80	19.917	307.15	1.914	3792.29	
98	5:00:50.64	-66:04:58.80	16.833	301.47	1.123	1775.11	
99	5:01:11.28	-67:32:34.80	15.870	252.01	1.518	3146.79	
100	5:01:31.92	-66:07:15.60	20.101	302.92	1.435	2662.67	
101	5:01:38.64	-66:24:39.60	60.302	302.75	3.155	41069.68	
102	5:01:38.64	-67:44:27.60	31.741	256.53	2.246	10327.94	
103	5:02:06.24	-66:57:32.40	254.130	290.80	6.867	1100086.56	
104	5:02:13.20	-67:18:28.80	26.753	249.64	3.251	5406.03	
105	5:02:26.88	-71:29:52.80	35.487	247.13	1.954	4518.47	
106	5:02:33.60	-71:37:04.80	34.589	244.02	1.725	5567.40	
107	5:02:47.52	-68:03:25.20	27.488	261.55	2.880	13716.79	
108	5:03:01.20	-67:55:37.20	39.913	293.38	1.794	8472.14	

Table 2—Continued

ID	RA (J2000)	DEC (J2000)	SIZE (pc)	Vel (kms ⁻¹)	σ (kms ⁻¹)	M_{cloud} (M_{\odot})	REGION
109	5:03:08.16	-66:25:33.60	21.683	296.76	1.077	2339.92	
110	5:03:14.88	-67:22:08.40	17.325	292.47	1.383	2097.86	
111	5:03:35.52	-66:03:36.00	15.366	294.00	1.000	1210.31	
112	5:03:35.52	-71:44:42.00	86.526	240.96	2.679	39133.19	
113	5:03:42.48	-67:46:12.00	41.397	298.35	2.741	23641.29	
114	5:03:42.48	-66:06:43.20	15.969	304.20	1.545	2420.61	
115	5:04:03.12	-71:34:08.40	50.124	246.82	2.658	10892.75	
116	5:04:16.80	-70:41:45.60	25.713	246.44	2.978	8633.51	
117	5:04:16.80	-71:22:22.80	28.611	250.22	1.891	5728.78	
118	5:04:16.80	-68:20:02.40	31.840	263.70	2.268	11376.87	
119	5:04:37.44	-65:20:45.60	15.936	293.20	0.981	1452.37	
120	5:04:44.40	-68:06:50.40	89.519	263.91	5.056	108524.01	
121	5:04:51.36	-67:18:07.20	23.135	301.89	2.588	4357.10	
122	5:05:12.00	-68:33:14.40	15.056	243.19	1.692	1775.11	End of Bar
123	5:05:18.72	-70:46:22.80	39.926	250.19	2.499	14039.54	
124	5:05:25.68	-68:09:00.00	60.632	296.19	2.815	24125.41	
125	5:05:32.64	-71:39:32.40	53.955	245.27	2.471	8391.45	
126	5:05:32.64	-69:48:54.00	17.325	246.75	0.433	1210.31	End of Bar
127	5:05:32.64	-67:52:01.20	38.330	269.67	2.860	18396.64	
128	5:05:39.36	-68:16:26.40	23.805	295.65	1.305	2662.67	
129	5:05:46.32	-68:59:31.20	20.386	275.45	3.401	3711.60	End of Bar
130	5:05:53.28	-71:36:43.20	21.755	239.97	1.000	1694.43	
131	5:06:00.24	-67:30:18.00	15.570	294.28	1.568	1936.49	
132	5:06:00.24	-71:00:57.60	104.129	246.01	4.146	63177.92	
133	5:06:00.24	-71:47:27.60	24.693	243.98	1.325	2581.98	
134	5:06:20.88	-66:40:48.00	21.243	284.22	1.773	2824.05	
135	5:06:20.88	-69:13:04.80	14.009	265.18	2.150	3066.11	End of Bar
136	5:06:27.60	-66:48:14.40	17.979	284.61	0.792	1371.68	
137	5:06:27.60	-66:15:36.00	40.332	300.28	3.159	19042.13	
138	5:06:34.56	-67:37:15.60	22.907	287.56	2.726	5163.97	
139	5:06:34.56	-68:32:02.40	50.851	242.38	3.548	25658.47	End of Bar
140	5:06:34.56	-68:47:09.60	15.870	262.75	1.875	2097.86	End of Bar
141	5:06:41.52	-71:33:25.20	32.524	235.98	1.607	7181.14	
142	5:06:55.20	-66:10:19.20	19.165	302.02	1.727	3308.17	
143	5:06:55.20	-70:27:14.40	31.039	231.82	2.975	9521.07	
144	5:06:55.20	-70:27:50.40	18.610	254.14	1.415	3308.17	

Table 2—Continued

ID	RA (J2000)	DEC (J2000)	SIZE (pc)	Vel (kms ⁻¹)	σ (kms ⁻¹)	M_{cloud} (M_{\odot})	REGION
145	5:07:02.16	-69:06:07.20	20.075	296.85	1.774	3469.54	End of Bar
146	5:07:09.12	-65:17:09.60	40.332	285.55	1.340	5325.34	
147	5:07:09.12	-68:31:40.80	21.755	221.57	2.204	3630.91	End of Bar
148	5:07:16.08	-68:25:37.20	40.188	223.11	3.601	17912.51	
149	5:07:16.08	-71:26:31.20	88.077	248.02	2.055	28159.76	
150	5:07:22.80	-68:17:49.20	33.195	218.85	3.718	19606.94	
151	5:07:36.72	-68:15:28.80	21.489	291.33	2.400	8068.70	
152	5:07:36.72	-66:08:09.60	22.537	303.62	1.844	3308.17	
153	5:07:36.72	-68:08:09.60	30.286	254.86	3.131	17831.83	
154	5:07:43.44	-65:49:40.80	72.293	292.98	1.667	26868.77	
155	5:07:43.44	-68:51:54.00	18.037	267.55	1.712	2501.30	End of Bar
156	5:07:50.40	-70:09:03.60	247.769	241.56	5.111	400853.02	
157	5:08:18.00	-67:54:28.80	65.057	291.79	2.556	41715.18	
158	5:08:31.92	-68:52:48.00	19.545	290.81	1.858	4437.78	End of Bar
159	5:08:38.64	-68:01:55.20	23.405	294.18	1.389	3227.48	
160	5:08:38.64	-69:24:14.40	87.844	245.05	4.458	208737.27	End of Bar
161	5:08:38.64	-66:00:-0.00	41.461	296.11	1.418	7261.83	
162	5:08:52.56	-71:25:15.60	17.861	242.47	1.132	1855.80	
163	5:09:06.24	-71:00:54.00	16.133	241.87	1.082	1775.11	
164	5:09:13.20	-71:12:54.00	34.452	224.95	1.913	7665.27	
165	5:09:13.20	-70:24:28.80	49.682	235.16	3.380	17186.33	
166	5:09:20.16	-64:59:31.20	30.286	294.25	1.637	7745.95	
167	5:09:20.16	-71:19:26.40	16.262	243.59	1.488	1533.05	
168	5:09:20.16	-70:46:04.80	148.884	239.54	2.864	109411.57	
169	5:09:27.12	-71:04:37.20	28.684	235.79	3.498	11538.24	
170	5:09:34.08	-66:26:52.80	19.518	302.50	1.734	3872.98	
171	5:09:34.08	-71:20:06.00	23.893	232.06	2.392	4679.85	
172	5:09:47.76	-67:53:13.20	19.891	289.45	1.688	2743.36	
173	5:09:54.72	-71:49:22.80	110.695	243.17	2.834	99809.82	
174	5:10:01.68	-71:16:04.80	27.659	230.40	1.198	2824.05	
175	5:10:08.40	-67:17:20.40	14.774	312.56	1.380	1936.49	
176	5:10:08.40	-71:30:25.20	27.488	243.09	2.240	6454.96	
177	5:10:15.36	-67:00:18.00	271.308	301.33	4.771	1103233.35	
178	5:10:15.36	-70:02:06.00	26.556	236.53	1.269	2581.98	
179	5:10:15.36	-67:53:24.00	22.746	314.64	2.795	8633.51	
180	5:10:36.24	-71:42:25.20	25.260	238.05	2.489	8472.14	

Table 2—Continued

ID	RA (J2000)	DEC (J2000)	SIZE (pc)	Vel (kms ⁻¹)	σ (kms ⁻¹)	M_{cloud} (M_{\odot})	REGION
181	5:10:36.24	-68:34:48.00	16.833	259.49	1.412	2097.86	End of Bar
182	5:10:42.96	-71:28:12.00	17.111	246.26	0.438	1129.62	
183	5:11:03.84	-71:35:27.60	35.928	242.01	1.996	10005.19	
184	5:11:31.44	-66:28:48.00	42.238	306.66	2.033	8794.88	
185	5:11:38.40	-66:53:24.00	20.283	296.12	0.993	2178.55	
186	5:11:52.08	-66:54:43.20	23.628	285.09	1.971	4115.04	
187	5:11:52.08	-67:03:18.00	32.265	279.72	2.619	10812.06	
188	5:11:59.04	-67:49:40.80	24.047	294.62	1.808	4276.41	
189	5:12:06.00	-67:16:48.00	20.994	314.71	1.165	3066.11	
190	5:12:19.68	-71:41:42.00	64.571	238.30	3.368	33969.23	Southern Arm
191	5:12:33.60	-67:32:49.20	226.988	303.54	7.068	1063454.66	
192	5:12:33.60	-72:00:07.20	31.207	231.59	1.666	5648.09	
193	5:12:40.56	-69:02:02.40	590.915	264.53	16.962	3060457.91	
194	5:12:47.52	-66:51:18.00	43.160	276.68	1.990	10166.56	
195	5:12:54.48	-71:29:56.40	91.982	240.33	2.562	63500.67	Southern Arm
196	5:12:54.48	-70:51:14.40	89.072	238.15	2.144	43167.54	
197	5:12:54.48	-66:26:13.20	90.335	303.20	2.642	48250.83	
198	5:12:54.48	-70:29:09.60	129.844	246.03	3.631	198893.45	
199	5:13:08.16	-71:07:22.80	131.254	235.04	3.824	227214.59	Southern Arm
200	5:13:15.12	-66:51:28.80	26.870	302.44	1.467	4760.53	
201	5:13:15.12	-68:47:06.00	62.574	279.18	3.999	35421.59	
202	5:13:22.08	-68:46:30.00	17.744	231.84	1.466	2743.36	
203	5:13:35.76	-68:41:06.00	18.468	292.49	1.315	2420.61	
204	5:14:03.60	-72:00:28.80	73.645	230.36	2.414	20736.56	
205	5:14:10.56	-71:20:09.60	14.632	234.69	1.806	2904.73	Southern Arm
206	5:14:17.28	-66:16:44.40	22.019	298.63	1.099	2339.92	
207	5:14:17.28	-70:12:43.20	65.930	253.00	3.415	72456.93	
208	5:14:24.24	-67:53:24.00	82.592	307.48	5.756	36470.52	
209	5:14:45.12	-71:23:13.20	31.641	236.67	1.106	5244.65	Southern Arm
210	5:14:52.08	-66:39:39.60	70.455	301.05	2.132	31225.87	
211	5:14:58.80	-66:11:24.00	37.106	300.92	1.782	7907.33	
212	5:15:26.64	-67:34:48.00	16.645	307.52	1.322	2339.92	
213	5:15:26.64	-70:36:18.00	41.989	234.89	2.164	10247.25	
214	5:15:40.32	-68:43:22.80	76.304	293.36	7.556	160083.01	
215	5:16:01.20	-69:46:08.40	34.815	261.69	2.515	8230.07	
216	5:16:21.84	-71:36:36.00	28.793	233.95	1.715	5083.28	Southern Arm

Table 2—Continued

ID	RA (J2000)	DEC (J2000)	SIZE (pc)	Vel (kms ⁻¹)	σ (kms ⁻¹)	M_{cloud} (M_{\odot})	REGION
217	5:16:21.84	-68:52:01.20	90.492	243.12	5.752	61564.18	
218	5:16:28.80	-69:04:40.80	49.172	237.43	3.003	16944.27	
219	5:16:28.80	-67:29:31.20	18.297	297.10	1.408	3550.23	
220	5:16:35.76	-68:57:28.80	24.778	244.51	3.543	7503.89	
221	5:16:35.76	-71:51:25.20	225.860	238.15	4.585	221566.50	Southern Arm
222	5:17:10.32	-67:06:25.20	27.792	307.96	1.014	3388.85	
223	5:17:17.28	-66:12:28.80	15.936	307.13	1.516	2259.24	
224	5:17:24.24	-68:46:08.40	22.350	305.07	2.644	8310.76	
225	5:17:24.24	-68:18:18.00	55.034	281.93	3.274	15653.28	
226	5:17:31.20	-69:45:46.80	21.683	254.41	1.847	5002.59	
227	5:17:38.16	-66:37:44.40	24.988	293.97	2.507	8149.39	
228	5:17:45.12	-68:35:56.40	48.202	287.63	3.323	17751.14	
229	5:17:45.12	-69:02:27.60	77.681	267.93	4.658	78508.45	
230	5:17:45.12	-69:59:34.80	94.375	264.20	3.676	111993.56	
231	5:17:45.12	-68:47:60.00	23.937	269.02	4.229	7342.52	
232	5:17:58.80	-68:46:12.00	32.621	297.17	4.737	10812.06	
233	5:18:05.76	-71:33:14.40	48.560	233.45	2.259	14846.41	Southern Arm
234	5:18:12.72	-71:15:25.20	117.791	238.88	3.653	129421.95	Southern Arm
235	5:18:40.56	-68:20:16.80	20.994	265.22	4.306	8310.76	
236	5:18:47.52	-68:46:19.20	14.845	297.63	1.406	2097.86	
237	5:19:15.12	-66:56:20.40	17.142	303.47	1.092	1775.11	
238	5:19:15.12	-70:20:42.00	21.144	251.49	1.165	2985.42	
239	5:19:15.12	-69:28:33.60	17.445	278.64	3.871	6293.59	
240	5:19:22.08	-68:24:00.00	70.989	297.11	3.137	36389.84	
241	5:19:22.08	-65:46:19.20	23.180	294.44	2.908	5728.78	
242	5:19:22.08	-69:50:09.60	58.795	242.57	2.855	18638.70	
243	5:19:36.00	-68:51:50.40	18.917	283.53	1.610	2581.98	
244	5:19:36.00	-68:20:24.00	25.713	252.91	1.377	3711.60	
245	5:19:49.68	-70:43:26.40	114.075	240.73	4.327	111670.81	
246	5:20:17.52	-70:22:37.20	22.792	246.25	1.354	3469.54	
247	5:20:24.48	-71:31:04.80	19.864	234.30	1.266	1936.49	Southern Arm
248	5:20:45.12	-68:12:00.00	45.203	238.61	2.228	17670.45	
249	5:20:59.04	-70:14:16.80	32.184	239.96	1.818	3227.48	
250	5:21:06.00	-65:54:28.80	22.019	302.24	1.734	4357.10	
251	5:21:06.00	-70:19:04.80	19.518	243.35	1.740	4115.04	
252	5:21:06.00	-69:32:56.40	18.917	270.88	2.822	7665.27	

Table 2—Continued

ID	RA (J2000)	DEC (J2000)	SIZE (pc)	Vel (kms ⁻¹)	σ (kms ⁻¹)	M_{cloud} (M_{\odot})	REGION
253	5:21:12.96	-69:59:56.40	153.800	253.21	5.845	203573.30	
254	5:21:26.88	-71:20:27.60	32.508	238.78	2.127	9601.75	Southern Arm
255	5:21:26.88	-65:16:12.00	45.063	303.94	1.626	15653.28	
256	5:21:40.56	-71:13:55.20	49.861	239.27	1.691	8794.88	Southern Arm
257	5:21:40.56	-69:05:52.80	17.979	273.02	1.580	2017.17	
258	5:21:47.52	-69:42:32.40	57.986	260.60	6.214	78750.51	
259	5:21:47.52	-69:09:28.80	49.650	275.49	5.083	24206.10	
260	5:21:47.52	-69:21:32.40	26.037	271.03	2.300	11054.12	
261	5:22:22.32	-65:37:19.20	103.208	308.52	4.177	242625.81	
262	5:22:22.32	-70:25:40.80	21.218	239.68	1.705	4760.53	
263	5:22:42.96	-67:44:13.20	12.250	302.44	3.359	4841.22	
264	5:22:49.92	-68:45:25.20	53.073	256.28	3.273	32678.24	
265	5:22:56.88	-67:38:42.00	17.325	306.19	1.212	1694.43	LMC4
266	5:23:03.84	-67:54:32.40	17.655	238.03	1.602	2017.17	
267	5:23:10.80	-70:47:45.60	29.937	240.14	1.192	3630.91	
268	5:23:10.80	-69:48:36.00	30.286	265.36	2.863	13636.10	
269	5:23:31.44	-65:31:08.40	26.017	312.91	1.295	4599.16	
270	5:23:38.40	-68:41:45.60	34.007	272.62	6.227	16621.52	
271	5:23:45.36	-70:36:28.80	37.219	246.60	2.547	13232.67	
272	5:24:06.24	-70:28:04.80	25.343	249.72	1.970	5567.40	
273	5:24:06.24	-72:41:34.80	18.610	250.81	0.964	1452.37	
274	5:24:13.20	-66:19:12.00	442.968	307.06	6.264	3759610.77	LMC4
275	5:24:13.20	-67:32:38.40	31.492	293.14	3.073	5163.97	LMC4
276	5:24:13.20	-70:59:42.00	26.831	239.59	1.583	5567.40	
277	5:24:19.92	-69:40:12.00	66.272	277.85	8.769	144671.79	
278	5:24:40.80	-72:39:14.40	26.318	251.09	1.024	3630.91	
279	5:24:54.72	-72:21:32.40	18.610	254.17	0.958	2097.86	
280	5:25:01.68	-70:41:49.20	22.019	243.11	0.994	2259.24	
281	5:25:22.32	-67:42:57.60	18.182	284.37	1.492	1694.43	
282	5:25:29.28	-65:34:08.40	22.998	311.01	1.862	7019.77	
283	5:25:29.28	-69:52:08.40	42.977	266.61	3.900	43248.23	
284	5:25:43.20	-67:59:56.40	18.297	290.48	2.386	4115.04	
285	5:26:04.08	-72:31:30.00	16.833	257.26	2.442	2259.24	
286	5:26:10.80	-68:56:09.60	61.908	253.64	2.225	25739.15	
287	5:26:10.80	-72:36:46.80	26.909	254.93	0.999	3630.91	
288	5:26:10.80	-72:15:32.40	34.314	262.82	0.984	2824.05	

Table 2—Continued

ID	RA (J2000)	DEC (J2000)	SIZE (pc)	Vel (kms ⁻¹)	σ (kms ⁻¹)	M_{cloud} (M_{\odot})	REGION
289	5:26:24.72	-68:38:38.40	17.655	281.83	1.371	2904.73	
290	5:26:24.72	-70:31:33.60	18.610	235.46	0.889	1129.62	
291	5:26:24.72	-70:52:26.40	28.647	241.12	2.105	4921.91	
292	5:26:24.72	-72:04:19.20	18.440	263.19	0.981	1371.68	
293	5:26:38.64	-68:06:32.40	38.330	287.11	2.950	25658.47	
294	5:26:38.64	-72:26:09.60	40.977	257.15	2.032	6777.71	
295	5:26:45.60	-67:15:25.20	37.388	311.66	3.088	24367.47	LMC4
296	5:26:59.52	-70:55:22.80	22.280	232.00	3.210	5728.78	
297	5:27:06.24	-71:56:34.80	64.245	227.53	2.400	19849.00	Southern Arm
298	5:27:20.16	-66:49:04.80	16.988	294.20	1.735	3308.17	LMC4
299	5:27:20.16	-70:27:57.60	127.416	248.38	3.266	78669.82	
300	5:27:27.12	-71:22:08.40	448.605	238.39	5.220	2348798.57	Southern Arm
301	5:27:27.12	-70:01:37.20	48.387	269.08	3.333	16460.15	
302	5:27:34.08	-71:48:50.40	31.375	260.33	1.431	3792.29	Southern Arm
303	5:28:01.68	-70:09:57.60	58.867	264.80	5.463	34776.10	
304	5:28:22.56	-71:53:27.60	46.833	235.78	1.710	11699.61	Southern Arm
305	5:28:29.52	-69:03:10.80	46.099	258.68	4.463	55916.09	
306	5:28:29.52	-71:44:34.80	22.677	272.86	0.990	1936.49	Southern Arm
307	5:28:43.44	-66:07:08.40	19.705	291.10	1.952	4276.41	LMC4
308	5:29:24.96	-69:53:34.80	17.325	288.13	2.506	4276.41	
309	5:29:52.56	-70:55:04.80	16.133	241.96	2.319	3469.54	
310	5:30:06.48	-68:01:51.60	18.778	279.17	1.598	3550.23	
311	5:30:06.48	-70:06:39.60	26.118	264.48	2.267	6858.40	
312	5:30:27.12	-67:45:25.20	15.870	289.85	3.396	5890.15	
313	5:31:15.60	-71:49:33.60	32.718	237.42	2.484	5486.72	Southern Arm
314	5:31:36.48	-67:32:24.00	17.445	300.57	1.675	2581.98	LMC4
315	5:32:11.04	-67:20:38.40	50.437	315.60	2.021	29773.50	LMC4
316	5:32:11.04	-69:47:06.00	50.374	280.35	3.807	39375.26	
317	5:32:45.60	-72:24:10.80	18.610	228.01	1.000	1129.62	
318	5:33:20.16	-71:02:13.20	29.549	248.28	2.700	6858.40	Southern Arm
319	5:33:20.16	-71:58:37.20	18.297	246.81	1.167	1371.68	Southern Arm
320	5:33:27.12	-70:40:08.40	15.969	272.76	1.608	1452.37	
321	5:33:34.08	-71:03:21.60	33.321	287.61	2.133	8633.51	Southern Arm
322	5:33:34.08	-69:39:00.00	19.705	260.85	2.244	5244.65	
323	5:33:34.08	-69:21:32.40	12.121	264.66	3.917	4679.85	
324	5:33:54.96	-69:53:56.40	19.220	252.65	1.367	1694.43	

Table 2—Continued

ID	RA (J2000)	DEC (J2000)	SIZE (pc)	Vel (kms ⁻¹)	σ (kms ⁻¹)	M_{cloud} (M_{\odot})	REGION
325	5:33:54.96	-68:47:42.00	20.231	255.77	1.631	2339.92	
326	5:34:50.16	-69:42:14.40	38.739	284.23	3.108	13232.67	
327	5:34:57.12	-70:45:43.20	56.035	235.03	2.428	13071.29	
328	5:35:04.08	-67:51:32.40	21.489	281.64	1.523	3953.66	
329	5:35:04.08	-70:48:03.60	29.335	284.32	3.259	6777.71	
330	5:35:10.80	-68:19:30.00	16.833	309.42	1.684	2824.05	
331	5:35:17.76	-68:28:30.00	19.220	277.76	1.657	2904.73	
332	5:35:24.72	-68:27:54.00	69.109	296.98	2.687	32274.80	
333	5:36:06.24	-67:15:14.40	14.739	310.76	1.584	1452.37	LMC4
334	5:36:33.84	-71:10:19.20	18.917	258.15	1.520	2259.24	Southern Arm
335	5:36:47.76	-66:10:33.60	33.666	301.53	2.736	19687.63	LMC4
336	5:37:08.40	-66:15:57.60	40.332	310.36	2.673	16540.83	LMC4
337	5:37:49.92	-71:20:02.40	19.165	237.98	1.769	3227.48	Southern Arm
338	5:37:49.92	-68:30:07.20	36.936	277.19	1.939	9924.50	30 Dor
339	5:37:56.64	-66:12:32.40	365.362	305.76	5.247	1248469.95	LMC4
340	5:38:10.56	-72:23:27.60	38.685	271.98	2.513	8472.14	
341	5:38:17.52	-67:11:20.40	22.091	291.82	2.023	3872.98	LMC4
342	5:38:24.24	-69:17:38.40	1499.823	270.82	23.292	49900794.46	30 Dor
343	5:38:38.16	-67:53:20.40	20.667	279.68	1.659	2017.17	
344	5:38:38.16	-67:00:50.40	39.437	290.79	3.479	20897.93	LMC4
345	5:38:45.12	-71:28:04.80	21.489	264.71	1.973	3872.98	Southern Arm
346	5:38:51.84	-66:49:04.80	36.765	317.70	2.940	15088.47	LMC4
347	5:38:51.84	-71:34:01.20	25.916	242.90	0.995	2501.30	Southern Arm
348	5:39:26.40	-71:39:10.80	28.167	237.38	4.740	7826.64	Southern Arm
349	5:39:40.32	-71:56:52.80	30.303	247.13	1.022	4518.47	Southern Arm
350	5:39:40.32	-66:41:20.40	33.976	269.88	2.483	8794.88	LMC4
351	5:39:47.04	-71:51:28.80	25.713	244.28	1.745	3711.60	Southern Arm
352	5:40:14.64	-67:52:04.80	22.907	287.72	1.568	3792.29	
353	5:40:14.64	-71:46:01.20	20.101	275.20	1.978	3872.98	
354	5:40:21.60	-70:38:34.80	45.584	280.74	2.156	14523.66	Southern Arm
355	5:40:21.60	-71:51:18.00	37.304	268.51	3.841	15895.34	
356	5:40:28.56	-67:03:03.60	96.742	290.65	3.544	57610.52	
357	5:40:35.28	-71:37:33.60	27.142	266.79	4.970	7907.33	
358	5:40:42.24	-67:45:46.80	32.395	295.23	2.239	12022.36	
359	5:40:56.16	-71:42:46.80	76.586	239.08	3.872	49299.76	
360	5:41:16.80	-70:44:49.20	18.610	277.34	1.391	1775.11	Southern Arm

Table 2—Continued

ID	RA (J2000)	DEC (J2000)	SIZE (pc)	Vel (kms ⁻¹)	σ (kms ⁻¹)	M_{cloud} (M_{\odot})	REGION
361	5:41:23.52	-71:05:06.00	35.796	257.72	2.757	10327.94	Southern Arm
362	5:41:23.52	-71:32:27.60	44.876	267.67	3.363	16379.46	
363	5:41:51.12	-70:27:46.80	48.916	280.24	1.281	6858.40	Southern Arm
364	5:41:51.12	-68:38:42.00	19.165	301.88	2.786	4115.04	30 Dor
365	5:41:51.12	-66:58:04.80	17.565	318.88	1.669	3953.66	
366	5:41:58.08	-67:34:08.40	24.501	293.84	3.582	7503.89	
367	5:41:58.08	-71:06:36.00	232.077	278.32	5.950	722471.40	Southern Arm
368	5:42:05.04	-68:11:16.80	26.258	278.75	5.137	9843.81	
369	5:42:18.72	-71:38:06.00	34.649	259.20	6.804	12829.23	
370	5:42:25.68	-66:45:32.40	25.997	300.59	2.297	10489.31	
371	5:42:32.40	-66:36:14.40	30.784	302.38	1.906	8794.88	
372	5:42:39.36	-67:49:04.80	32.395	294.68	2.908	5728.78	
373	5:42:46.32	-67:08:02.40	55.148	314.02	3.919	27514.27	
374	5:42:53.04	-67:25:08.40	29.955	306.71	1.919	6212.90	
375	5:43:00.00	-70:40:30.00	35.011	276.11	2.337	12425.80	Southern Arm
376	5:44:08.88	-70:07:33.60	23.893	285.90	1.772	3308.17	Southern Arm
377	5:44:08.88	-67:02:60.00	16.262	293.69	1.566	2581.98	
378	5:44:36.24	-69:50:27.60	32.233	291.52	3.098	7665.27	Southern Arm
379	5:44:36.24	-66:57:10.80	41.334	294.84	2.945	24770.91	
380	5:44:49.92	-71:58:22.80	18.325	297.24	0.429	1129.62	
381	5:44:56.88	-70:25:12.00	26.556	277.64	1.600	3146.79	Southern Arm
382	5:45:03.84	-67:33:43.20	15.056	296.15	2.755	3792.29	
383	5:46:05.52	-66:50:45.60	20.386	300.55	2.236	5002.59	
384	5:46:19.20	-68:19:58.80	15.969	324.21	2.527	2501.30	
385	5:47:07.20	-67:23:52.80	111.158	299.57	4.433	194213.61	
386	5:47:21.12	-67:37:12.00	46.405	295.62	4.023	31709.99	
387	5:47:27.84	-66:22:44.40	310.669	300.46	3.894	825266.64	
388	5:48:15.84	-67:04:40.80	59.909	297.19	4.015	67373.65	
389	5:48:22.80	-69:13:55.20	39.834	281.02	2.102	9440.38	
390	5:49:10.56	-69:06:10.80	21.342	279.16	1.403	3711.60	
391	5:49:17.52	-66:49:48.00	53.907	297.75	2.398	32597.55	
392	5:50:05.28	-67:38:24.00	40.384	285.50	1.958	16944.27	
393	5:50:12.24	-67:00:14.40	43.559	298.88	3.318	21301.37	
394	5:50:53.28	-69:11:42.00	15.366	289.98	1.775	1371.68	
395	5:50:60.00	-69:02:31.20	16.133	284.74	1.676	1936.49	
396	5:53:09.60	-69:11:16.80	18.889	323.01	1.507	1936.49	

Table 2—Continued

ID	RA (J2000)	DEC (J2000)	SIZE (pc)	Vel (kms ⁻¹)	σ (kms ⁻¹)	M_{cloud} (M_{\odot})	REGION
397	5:54:17.76	-69:08:02.40	38.262	301.60	1.838	12909.92	
398	5:54:31.44	-69:18:46.80	63.216	316.02	3.146	20010.38	
399	5:55:59.76	-68:45:57.60	20.231	300.61	2.734	6939.08	
400	5:56:13.44	-69:20:27.60	18.917	313.51	1.215	2259.24	
401	5:56:33.84	-69:25:04.80	45.492	313.55	1.205	9198.32	
402	5:56:40.56	-69:15:50.40	26.437	315.01	1.786	3711.60	
403	5:57:21.12	-68:01:19.20	24.134	311.09	1.408	4115.04	
404	5:59:16.32	-68:12:28.80	16.833	293.79	0.978	1371.68	
405	5:59:23.04	-68:06:14.40	20.101	304.29	1.485	2420.61	
406	6:00:03.60	-68:09:14.40	31.741	298.88	1.570	7342.52	

Table 3. Catalog of H I cloud for the brightness temperature threshold of 64 K

ID	RA (J2000)	DEC (J2000)	SIZE (pc)	Vel (kms ⁻¹)	σ (kms ⁻¹)	M_{cloud} (M_{\odot})	REGION
1	4:42:57.12	-68:41:56.40	18.945	256.27	1.382	4437.78	Northern Arm
2	4:43:37.44	-68:49:22.80	20.994	258.43	1.067	5163.97	Northern Arm
3	4:43:44.16	-67:15:10.80	44.371	272.13	1.500	16056.71	Northern Arm
4	4:44:51.36	-69:01:01.20	23.584	257.13	2.054	7503.89	Northern Arm
5	4:46:18.96	-68:19:33.60	19.917	273.55	1.040	4195.72	Northern Arm
6	4:46:59.52	-68:49:01.20	52.636	263.16	2.640	26303.96	Northern Arm
7	4:47:33.36	-69:15:46.80	15.536	251.83	1.068	3308.17	Northern Arm
8	4:48:13.92	-68:23:13.20	69.132	264.65	1.521	33807.85	Northern Arm
9	4:48:13.92	-66:56:24.00	94.891	291.22	3.603	324442.43	Northern Arm
10	4:48:20.64	-68:03:43.20	37.640	270.08	1.268	12022.36	Northern Arm
11	4:48:20.64	-67:18:43.20	24.501	290.24	2.041	5002.59	Northern Arm
12	4:48:54.48	-68:48:18.00	16.988	269.40	0.490	2743.36	Northern Arm
13	4:48:54.48	-67:13:44.40	26.118	290.92	1.562	8391.45	Northern Arm
14	4:49:14.88	-69:16:37.20	189.765	255.70	3.946	514944.43	Northern Arm
15	4:49:35.04	-69:41:49.20	24.988	250.69	1.196	7584.58	Northern Arm
16	4:50:02.16	-68:07:40.80	77.762	279.33	2.118	47605.33	Northern Arm
17	4:50:15.84	-69:00:25.20	59.672	263.89	3.185	75523.03	Northern Arm
18	4:50:42.96	-65:57:57.60	21.292	290.57	3.165	12183.74	Northern Arm
19	4:51:03.36	-66:17:34.80	88.273	288.75	4.004	228989.71	Northern Arm
20	4:51:57.84	-69:41:56.40	18.325	246.50	0.500	3388.85	Northern Arm
21	4:51:57.84	-70:55:33.60	25.855	253.71	1.196	9279.00	
22	4:52:31.68	-69:11:24.00	84.774	260.72	3.823	148383.39	Northern Arm
23	4:52:59.04	-69:30:00.00	34.815	252.54	1.314	10731.37	Northern Arm
24	4:53:12.48	-68:30:32.40	116.578	277.12	2.548	104086.23	Northern Arm
25	4:53:33.12	-68:24:43.20	21.731	279.72	1.464	5163.97	Northern Arm
26	4:53:39.84	-67:13:40.80	18.095	290.27	1.698	6212.90	Northern Arm
27	4:54:00.24	-69:30:07.20	50.333	248.13	2.437	28966.63	Northern Arm
28	4:54:00.24	-69:20:24.00	35.086	249.74	2.287	15814.65	Northern Arm
29	4:54:34.32	-66:15:07.20	220.487	292.79	4.550	1167540.89	Northern Arm
30	4:55:29.04	-68:27:21.60	24.264	272.38	1.708	9440.38	Northern Arm
31	4:55:42.72	-68:43:58.80	44.888	279.34	1.909	17670.45	Northern Arm
32	4:56:23.52	-68:52:58.80	30.733	274.90	3.047	12587.17	End of Bar
33	4:57:25.20	-66:19:15.60	28.055	291.16	1.557	10812.06	
34	4:57:59.28	-67:01:37.20	18.383	289.37	1.479	4599.16	
35	4:58:12.96	-69:07:33.60	31.475	262.73	2.440	15733.97	End of Bar
36	4:59:35.28	-65:52:19.20	44.853	295.65	2.794	47040.52	

Table 3—Continued

ID	RA (J2000)	DEC (J2000)	SIZE (pc)	Vel (kms ⁻¹)	σ (kms ⁻¹)	M_{cloud} (M_{\odot})	REGION
37	5:00:02.64	-68:57:07.20	34.038	281.34	2.104	25416.40	End of Bar
38	5:00:09.60	-70:10:51.60	20.616	242.16	2.105	7988.01	
39	5:00:57.60	-65:52:40.80	43.087	297.57	1.985	26707.40	
40	5:01:11.28	-67:08:02.40	49.523	285.03	3.940	48412.20	
41	5:01:38.64	-69:03:32.40	60.171	283.88	2.291	57529.83	End of Bar
42	5:01:38.64	-67:19:22.80	20.642	289.89	2.397	9036.94	
43	5:02:06.24	-65:45:21.60	24.629	300.65	0.938	5002.59	
44	5:02:13.20	-67:01:55.20	22.769	286.39	1.692	8794.88	
45	5:02:19.92	-66:51:32.40	38.874	292.14	2.982	21301.37	
46	5:02:54.24	-68:31:26.40	32.233	270.10	4.431	18558.01	End of Bar
47	5:03:42.48	-65:28:19.20	58.131	293.88	1.407	30096.25	
48	5:04:23.76	-69:07:22.80	34.589	288.26	1.531	14039.54	End of Bar
49	5:08:18.00	-68:26:42.00	30.903	287.61	1.879	18073.89	
50	5:08:24.96	-68:31:33.60	16.833	284.62	1.707	4599.16	End of Bar
51	5:08:52.56	-69:24:18.00	65.435	244.14	2.889	60353.88	End of Bar
52	5:08:59.52	-68:39:39.60	21.731	284.78	1.702	8310.76	End of Bar
53	5:09:13.20	-66:54:57.60	66.941	301.96	2.038	59224.26	
54	5:09:47.76	-69:12:36.00	17.979	252.13	1.693	5809.46	End of Bar
55	5:09:54.72	-70:18:07.20	25.322	237.99	1.441	8714.20	
56	5:10:01.68	-70:50:27.60	18.610	238.69	1.381	3388.85	
57	5:10:22.32	-67:44:16.80	20.231	295.64	1.484	4518.47	
58	5:10:49.92	-68:59:38.40	146.733	253.60	3.674	215595.66	End of Bar
59	5:10:56.88	-68:31:15.60	32.233	296.93	1.689	10892.75	End of Bar
60	5:10:56.88	-67:05:24.00	96.280	299.45	3.372	81977.99	
61	5:12:40.56	-69:20:06.00	29.691	247.95	2.548	13151.98	
62	5:12:47.52	-70:25:33.60	34.770	247.26	2.109	11538.24	
63	5:12:54.48	-69:38:13.20	67.332	249.90	2.851	63581.36	
64	5:13:01.20	-71:10:58.80	26.118	236.27	1.633	11699.61	Southern Arm
65	5:13:08.16	-67:29:56.40	79.087	305.38	4.499	144429.73	
66	5:13:22.08	-69:13:04.80	42.916	247.77	1.629	17912.51	
67	5:14:24.24	-70:12:10.80	29.335	252.70	1.810	12264.42	
68	5:14:52.08	-68:14:45.60	18.610	305.09	2.213	4357.10	
69	5:15:47.28	-68:44:02.40	19.437	290.73	1.706	6293.59	
70	5:15:47.28	-68:16:48.00	47.721	298.30	3.218	34211.29	
71	5:16:01.20	-68:08:20.40	28.975	297.79	2.301	12103.05	
72	5:16:08.16	-68:00:28.80	51.477	296.05	2.317	31145.18	

Table 3—Continued

ID	RA (J2000)	DEC (J2000)	SIZE (pc)	Vel (kms ⁻¹)	σ (kms ⁻¹)	M_{cloud} (M_{\odot})	REGION
73	5:16:56.64	-67:50:16.80	37.050	293.15	1.741	21543.43	
74	5:17:58.80	-71:16:37.20	29.084	238.70	1.786	5728.78	Southern Arm
75	5:18:47.52	-66:33:39.60	26.792	304.84	1.905	13555.42	
76	5:19:01.20	-67:40:15.60	29.424	306.71	1.425	8552.82	
77	5:19:08.16	-69:36:21.60	23.405	253.14	1.530	8633.51	
78	5:19:22.08	-66:31:51.60	20.101	302.42	0.494	3953.66	
79	5:19:36.00	-69:08:45.60	27.373	281.66	2.300	17670.45	
80	5:19:42.72	-66:39:14.40	33.353	305.93	1.784	11296.18	
81	5:20:03.60	-66:07:22.80	24.134	306.31	1.475	7503.89	
82	5:20:17.52	-66:46:40.80	59.381	307.16	2.110	40101.44	
83	5:20:31.44	-66:35:02.40	15.536	304.40	1.668	5325.34	
84	5:20:59.04	-68:46:33.60	32.200	297.21	3.058	18719.38	
85	5:21:06.00	-68:29:38.40	48.916	261.10	5.040	44942.66	
86	5:21:19.92	-68:08:24.00	14.845	306.77	1.962	5163.97	
87	5:22:08.40	-68:01:12.00	135.952	297.02	4.462	461529.64	
88	5:22:22.32	-65:39:46.80	50.447	309.51	2.387	30741.75	
89	5:22:29.04	-66:41:56.40	53.741	308.14	3.390	87706.77	LMC4
90	5:22:42.96	-67:07:37.20	53.965	305.07	3.926	102633.86	LMC4
91	5:23:24.48	-67:24:43.20	16.518	304.01	1.000	2178.55	LMC4
92	5:23:24.48	-66:23:31.20	19.220	319.00	1.540	5648.09	LMC4
93	5:23:38.40	-66:44:24.00	15.366	313.51	1.433	5325.34	LMC4
94	5:23:59.28	-68:22:26.40	127.996	269.29	5.869	359137.84	
95	5:24:19.92	-69:11:20.40	55.659	276.50	2.413	37680.83	
96	5:24:26.88	-69:23:56.40	22.815	268.75	1.085	4518.47	
97	5:24:26.88	-69:19:44.40	29.228	271.74	2.286	15169.16	
98	5:24:26.88	-67:27:07.20	27.181	302.70	2.266	18315.95	LMC4
99	5:24:33.84	-67:08:49.20	20.231	305.75	2.963	10247.25	LMC4
100	5:24:47.76	-69:39:36.00	17.325	273.85	3.010	5648.09	
101	5:24:54.72	-71:37:08.40	72.147	237.53	1.954	58336.70	Southern Arm
102	5:25:36.24	-67:08:49.20	25.405	305.78	2.079	9198.32	LMC4
103	5:25:43.20	-67:47:09.60	17.325	296.73	1.929	4518.47	
104	5:25:50.16	-68:14:31.20	15.936	268.87	1.235	4034.35	
105	5:26:10.80	-68:46:33.60	31.988	269.11	1.959	18315.95	
106	5:26:10.80	-66:15:25.20	178.556	306.84	4.984	1019641.62	LMC4
107	5:26:31.68	-65:47:42.00	35.324	309.01	2.382	25335.72	
108	5:26:31.68	-65:42:43.20	16.645	307.03	1.594	3872.98	

Table 3—Continued

ID	RA (J2000)	DEC (J2000)	SIZE (pc)	Vel (kms ⁻¹)	σ (kms ⁻¹)	M_{cloud} (M_{\odot})	REGION
109	5:26:45.60	-71:23:56.40	42.548	238.34	1.987	20413.81	Southern Arm
110	5:26:59.52	-67:50:06.00	35.339	291.76	1.600	8714.20	
111	5:27:27.12	-67:46:26.40	34.130	289.71	1.618	11296.18	
112	5:27:27.12	-67:33:39.60	22.067	292.61	2.152	11134.81	LMC4
113	5:27:27.12	-71:20:56.40	16.895	240.00	1.609	3872.98	Southern Arm
114	5:28:22.56	-70:57:03.60	24.565	237.58	2.317	8068.70	
115	5:28:29.52	-69:02:34.80	26.615	259.43	2.888	15491.90	
116	5:28:43.44	-68:09:21.60	23.717	274.85	2.411	15733.97	
117	5:28:43.44	-67:25:33.60	27.640	303.30	2.834	16540.83	LMC4
118	5:29:45.60	-68:24:21.60	25.260	267.34	1.632	7745.95	
119	5:30:13.44	-71:10:30.00	152.285	240.51	4.181	215676.35	Southern Arm
120	5:31:22.56	-69:09:21.60	19.811	257.96	2.209	7988.01	
121	5:32:31.92	-68:28:04.80	163.523	274.72	5.422	550366.03	
122	5:32:45.60	-67:45:28.80	143.588	298.42	4.237	356152.42	
123	5:33:06.48	-68:58:08.40	32.524	268.31	3.365	27675.64	
124	5:33:20.16	-69:03:32.40	18.917	267.81	1.473	5163.97	
125	5:33:20.16	-66:22:48.00	26.615	303.83	1.542	11780.30	LMC4
126	5:33:34.08	-66:01:48.00	44.888	310.53	1.529	19606.94	LMC4
127	5:34:08.64	-69:51:28.80	39.330	269.92	2.653	25739.15	
128	5:34:08.64	-67:29:16.80	18.297	293.80	1.656	4679.85	LMC4
129	5:34:43.20	-68:46:15.60	21.731	272.58	2.034	8230.07	30 Dor
130	5:34:50.16	-67:43:44.40	15.570	298.14	1.241	3953.66	
131	5:34:57.12	-69:32:02.40	16.133	270.49	2.504	6374.27	
132	5:35:17.76	-70:33:03.60	17.744	258.48	0.879	2178.55	
133	5:35:17.76	-68:09:43.20	74.860	292.15	3.154	56319.53	
134	5:35:52.32	-69:06:25.20	20.386	292.99	1.525	5648.09	30 Dor
135	5:35:59.28	-69:14:13.20	13.971	275.33	3.342	6212.90	30 Dor
136	5:36:13.20	-68:43:58.80	26.536	264.32	2.460	6212.90	30 Dor
137	5:37:08.40	-68:43:40.80	15.195	269.98	0.991	3388.85	30 Dor
138	5:37:08.40	-65:58:04.80	13.552	301.66	1.923	5244.65	LMC4
139	5:37:29.04	-67:37:19.20	18.297	291.73	2.044	3872.98	LMC4
140	5:37:36.00	-70:20:60.00	30.937	234.15	2.168	15653.28	Southern Arm
141	5:37:36.00	-70:27:00.00	34.038	256.96	3.484	33727.17	Southern Arm
142	5:37:49.92	-67:32:56.40	93.722	297.12	4.544	304512.74	LMC4
143	5:38:10.56	-69:08:42.00	225.141	269.68	7.738	866901.13	30 Dor
144	5:38:17.52	-69:14:06.00	18.917	280.77	1.397	4921.91	30 Dor

Table 3—Continued

ID	RA (J2000)	DEC (J2000)	SIZE (pc)	Vel (kms ⁻¹)	σ (kms ⁻¹)	M_{cloud} (M_{\odot})	REGION
145	5:38:17.52	-71:08:34.80	51.426	241.31	3.265	36954.65	Southern Arm
146	5:38:24.24	-71:29:24.00	22.327	222.71	1.162	3872.98	Southern Arm
147	5:39:05.76	-69:54:07.20	283.779	258.71	8.030	2913042.76	Southern Arm
148	5:39:05.76	-69:11:56.40	20.692	289.92	1.832	5970.84	30 Dor
149	5:39:12.72	-66:25:33.60	63.017	303.52	2.818	51639.68	LMC4
150	5:39:12.72	-66:17:34.80	17.655	303.76	1.981	7503.89	LMC4
151	5:39:33.36	-70:43:04.80	213.314	242.08	5.099	372693.25	Southern Arm
152	5:39:54.00	-71:17:34.80	43.099	227.91	2.807	30176.94	Southern Arm
153	5:40:00.96	-69:29:42.00	16.518	239.76	2.026	5083.28	Southern Arm
154	5:40:42.24	-69:28:12.00	17.714	263.16	2.081	6212.90	Southern Arm
155	5:40:56.16	-69:19:40.80	16.988	272.81	4.822	12183.74	30 Dor
156	5:41:23.52	-68:52:15.60	188.249	276.24	7.798	1495856.29	30 Dor
157	5:41:58.08	-71:00:03.60	39.596	277.47	3.455	33485.11	Southern Arm
158	5:42:32.40	-69:16:30.00	17.565	260.20	1.984	5244.65	30 Dor
159	5:43:00.00	-70:21:18.00	80.429	256.08	3.480	106829.59	Southern Arm
160	5:43:06.96	-70:47:38.40	33.100	238.62	3.787	18800.07	Southern Arm
161	5:43:06.96	-69:45:10.80	41.461	252.04	4.815	68664.64	Southern Arm
162	5:43:41.28	-69:03:54.00	33.243	259.87	1.820	12829.23	30 Dor
163	5:43:54.96	-70:38:16.80	46.609	237.35	2.942	26465.34	Southern Arm
164	5:44:01.92	-69:20:38.40	87.790	254.68	5.223	259408.70	30 Dor
165	5:44:15.60	-68:56:20.40	15.936	265.30	1.161	3872.98	30 Dor
166	5:44:43.20	-69:51:03.60	49.935	247.92	3.736	81332.50	Southern Arm
167	5:44:49.92	-68:51:46.80	15.332	282.87	1.642	3872.98	30 Dor
168	5:44:56.88	-68:55:58.80	15.195	265.02	1.011	3388.85	30 Dor
169	5:44:56.88	-68:14:38.40	36.277	299.44	2.712	31871.37	
170	5:45:03.84	-67:55:40.80	41.385	295.22	2.447	26303.96	
171	5:45:10.56	-69:36:57.60	22.746	251.14	2.781	13636.10	Southern Arm
172	5:45:38.16	-68:32:31.20	21.292	287.54	1.437	7342.52	
173	5:45:38.16	-66:24:32.40	46.338	301.35	1.741	23641.29	
174	5:46:32.88	-68:33:46.80	15.936	304.73	2.539	6939.08	
175	5:46:39.84	-66:40:33.60	17.979	299.38	1.482	4518.47	
176	5:46:46.80	-67:23:27.60	24.199	299.77	1.469	5002.59	
177	5:46:53.52	-69:47:27.60	148.736	244.12	5.055	381568.82	Southern Arm
178	5:46:53.52	-68:01:19.20	26.870	298.84	0.987	3872.98	
179	5:47:00.48	-69:23:13.20	84.749	245.63	4.549	104812.41	
180	5:47:41.52	-69:59:38.40	22.067	233.24	2.006	7261.83	Southern Arm

Table 3—Continued

ID	RA (J2000)	DEC (J2000)	SIZE (pc)	Vel (kms ⁻¹)	σ (kms ⁻¹)	M_{cloud} (M_{\odot})	REGION
181	5:47:41.52	-68:53:09.60	18.917	289.75	1.559	4518.47	
182	5:47:48.48	-69:27:00.00	19.811	229.32	1.630	5002.59	Southern Arm
183	5:48:02.16	-68:07:19.20	36.363	300.77	1.444	14846.41	
184	5:48:02.16	-66:11:49.20	54.747	302.70	1.904	51155.56	
185	5:48:56.88	-69:20:52.80	42.977	296.51	1.114	13313.35	
186	5:49:31.20	-68:59:52.80	19.437	298.44	4.866	12909.92	
187	5:49:51.60	-68:51:10.80	39.729	300.10	2.272	23641.29	
188	5:50:18.96	-69:14:31.20	45.997	305.63	1.205	7261.83	
189	5:50:53.28	-68:28:33.60	66.390	308.52	3.145	111106.00	
190	5:50:53.28	-68:42:32.40	17.142	308.01	0.993	3308.17	
191	5:51:34.08	-68:46:55.20	31.575	306.68	1.641	13797.48	
192	5:52:56.16	-68:27:03.60	34.710	312.98	2.253	24690.22	
193	5:54:38.16	-68:22:01.20	60.917	300.70	1.794	42764.11	
194	5:56:33.84	-68:10:01.20	18.610	294.60	0.798	2743.36	
195	5:57:21.12	-68:14:49.20	47.046	295.64	1.475	12425.80	

Table 4. Derived Parameters of the Mass Distributions

Parameter	$T_{thresh} = 64$ K	$T_{thresh} = 32$ K	$T_{thresh} = 16$ K
Power-Law Distributions			
Completeness Limit (M_{\odot})	10^4	5×10^3	2.5×10^3
N_0	22 ± 15	34 ± 16	5 ± 2
γ	-1.68 ± 0.04	-1.65 ± 0.04	-1.99 ± 0.04
Log-normal distribution.			
N_0	800 ± 200	1400 ± 150	810 ± 30
$\sigma_{\ln M}$	4.2 ± 0.3	4.1 ± 0.1	2.34 ± 0.04
$\ln(M_0/M_{\odot})$	5.9 ± 0.7	5.7 ± 0.3	6.8 ± 0.1

Table 5. Derived Parameters of the Column Density Distributions

Parameter	$T_{thresh} = 64$ K	$T_{thresh} = 32$ K	$T_{thresh} = 16$ K
N_0	200 ± 10	430 ± 20	480 ± 20
$\sigma_{\ln N(\text{H})}$	0.64 ± 0.05	0.78 ± 0.04	0.78 ± 0.04
$(N_{\text{H},0}/10^{20} \text{ cm}^{-2})$	6.0 ± 0.4	3.1 ± 0.3	1.6 ± 0.2

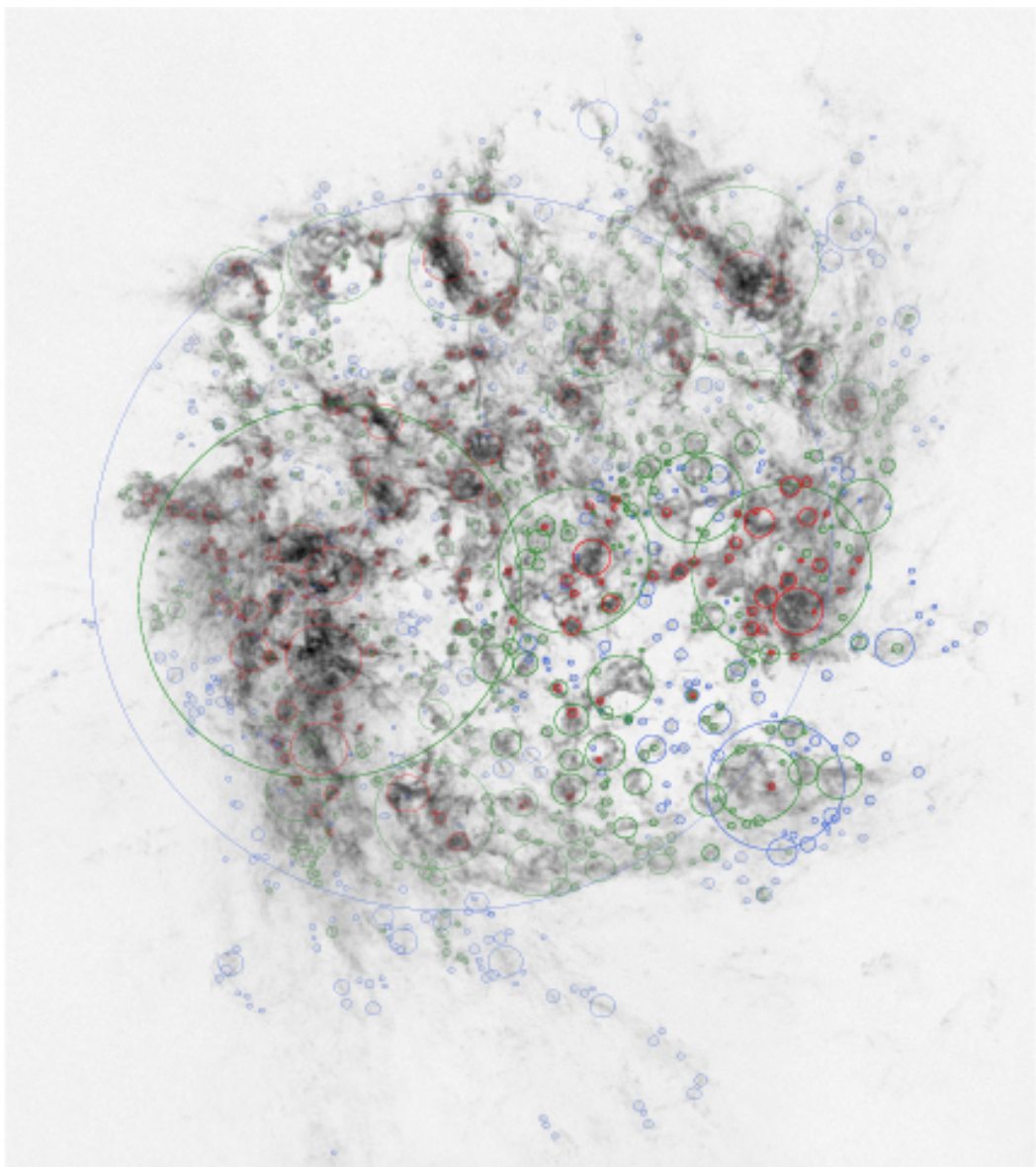


Fig. 1.— The size distribution of H I clouds in the LMC. Size of an ellipse presents size of H I cloud. Blue, green, and red colors represent brightness temperature threshold at 16 K, 32 K, and 64 K respectively.

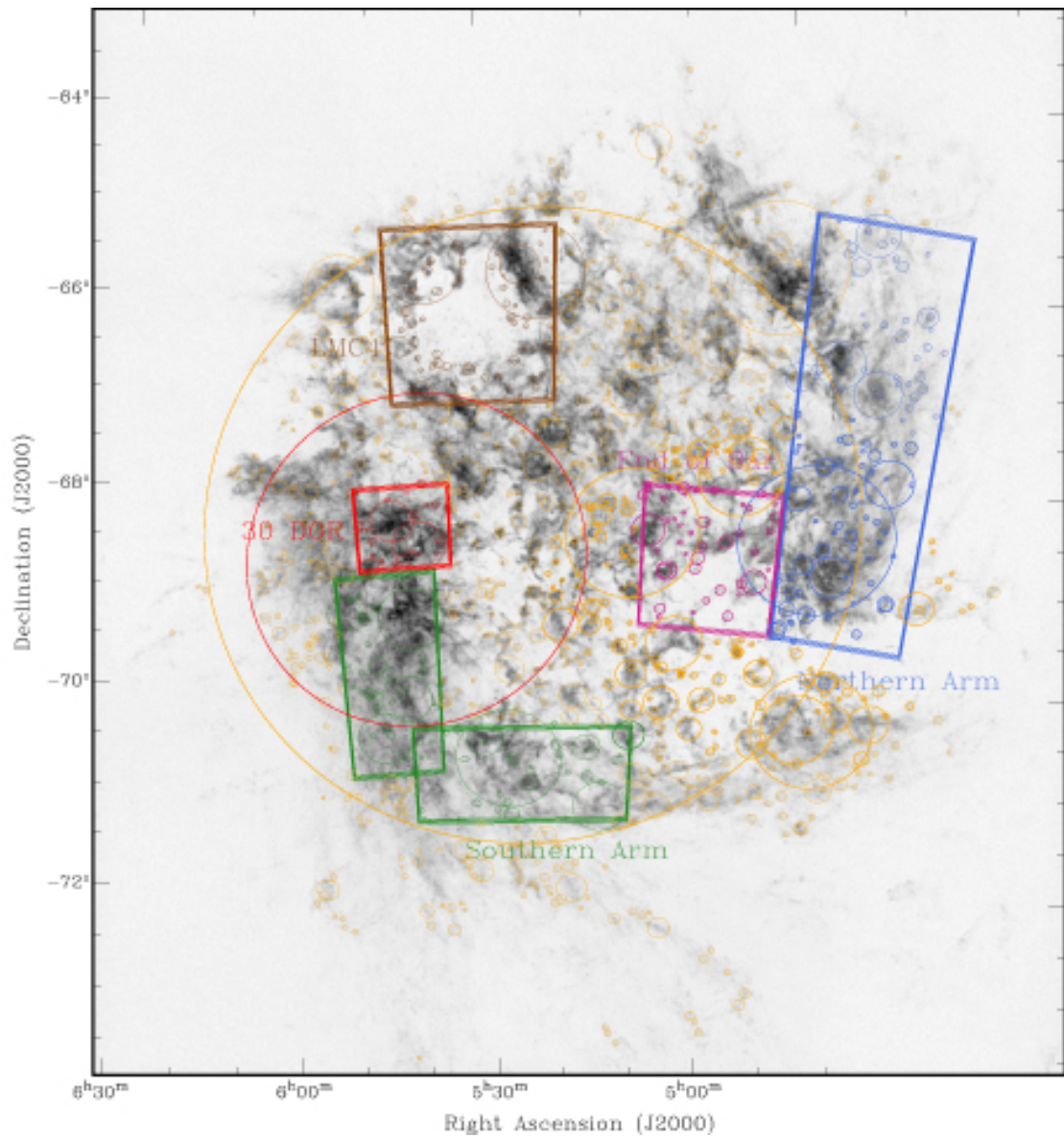


Fig. 2.— 2D spatial distribution and size distribution of clouds selected for each region.

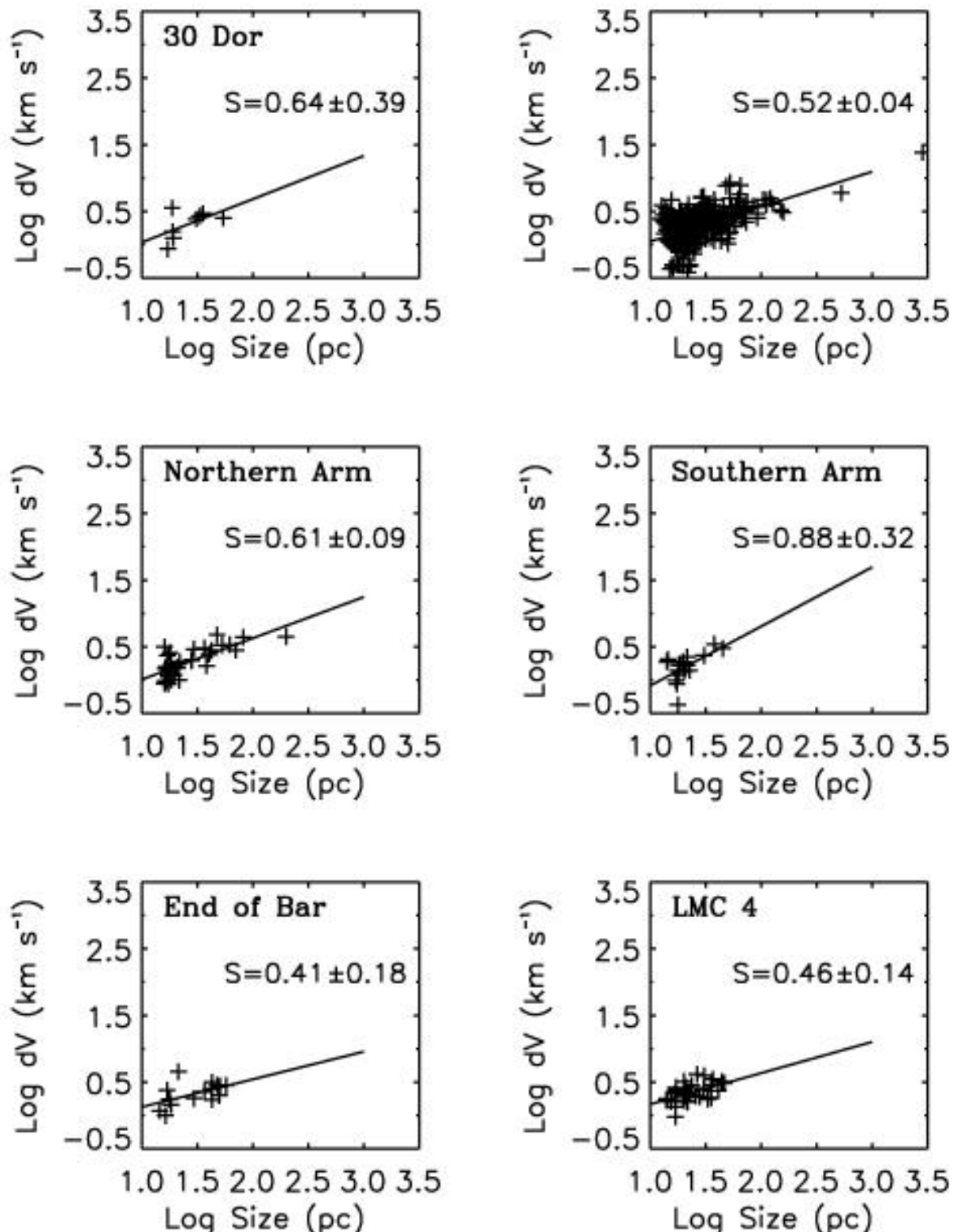


Fig. 3.— A plot of the size versus the velocity dispersion of H I cloud for each region ($T_b = 16K$). 30 Dor, Northern & Southern Spiral Arm, End of Bar, and the LMC 4 indicate the dynamically hot regions and the relatively quiet region is presented in the upper right panel.

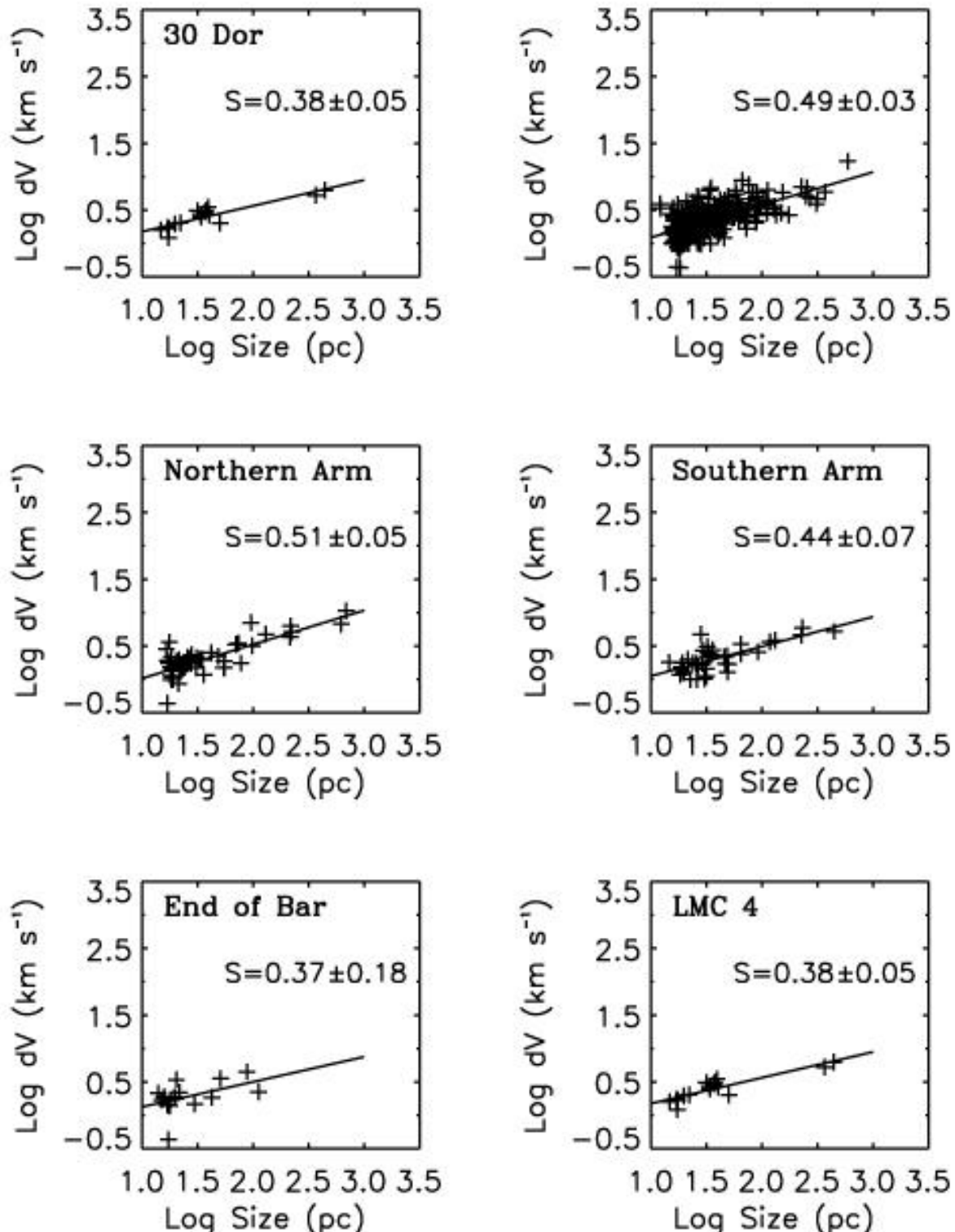


Fig. 4.— A plot of the size versus the velocity dispersion of H I cloud for each region ($T_b = 32K$). 30 Dor, Northern & Southern Spiral Arm, End of Bar, and the LMC 4 indicate the dynamically hot regions and the relatively quiet region is presented in the upper right panel.

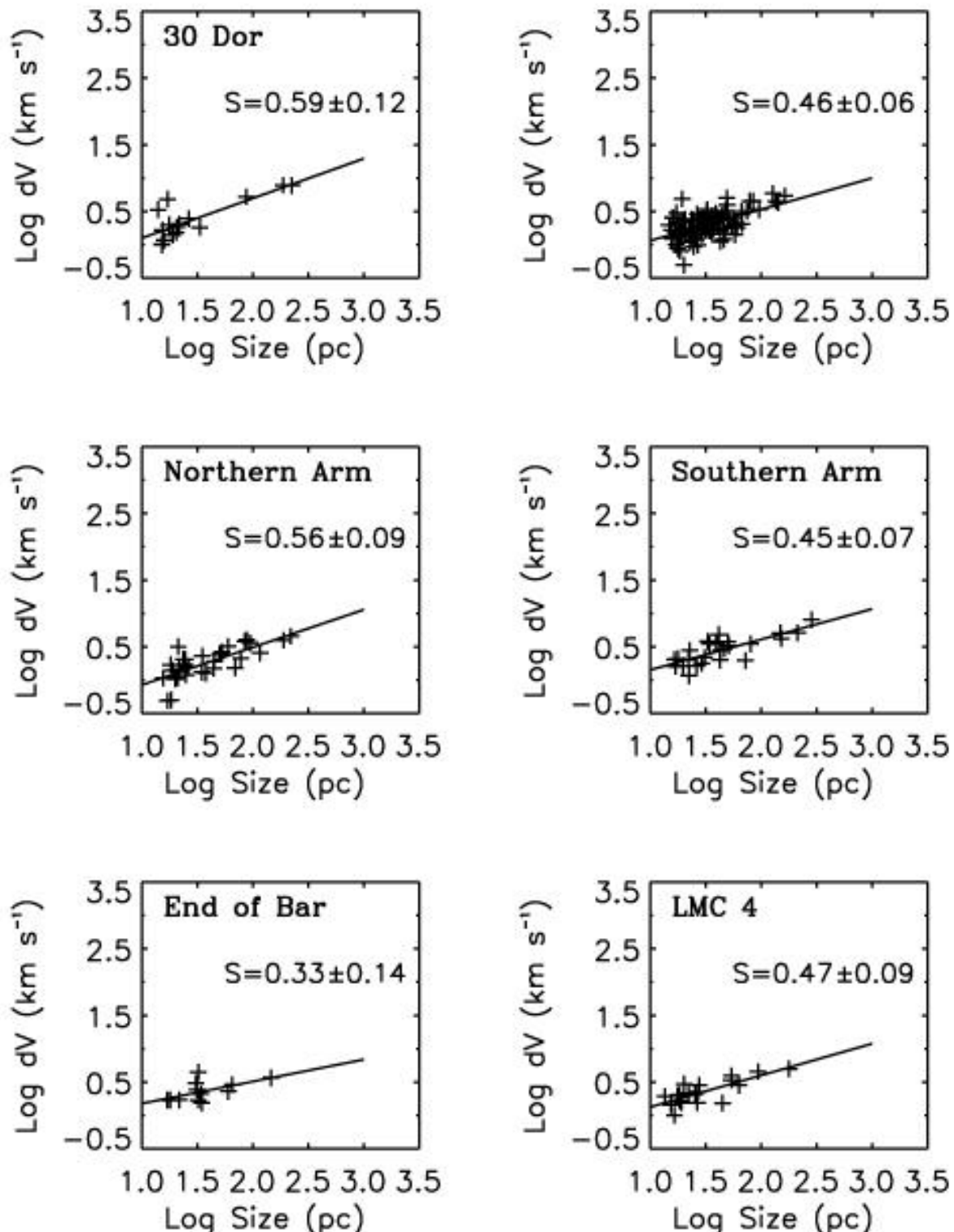


Fig. 5.— A plot of the size versus the velocity dispersion of H I cloud for each region ($T_b = 64K$). 30 Dor, Northern & Southern Spiral Arm, End of Bar, and the LMC 4 indicate the dynamically hot regions and the relatively quiet region is presented in the upper right panel.

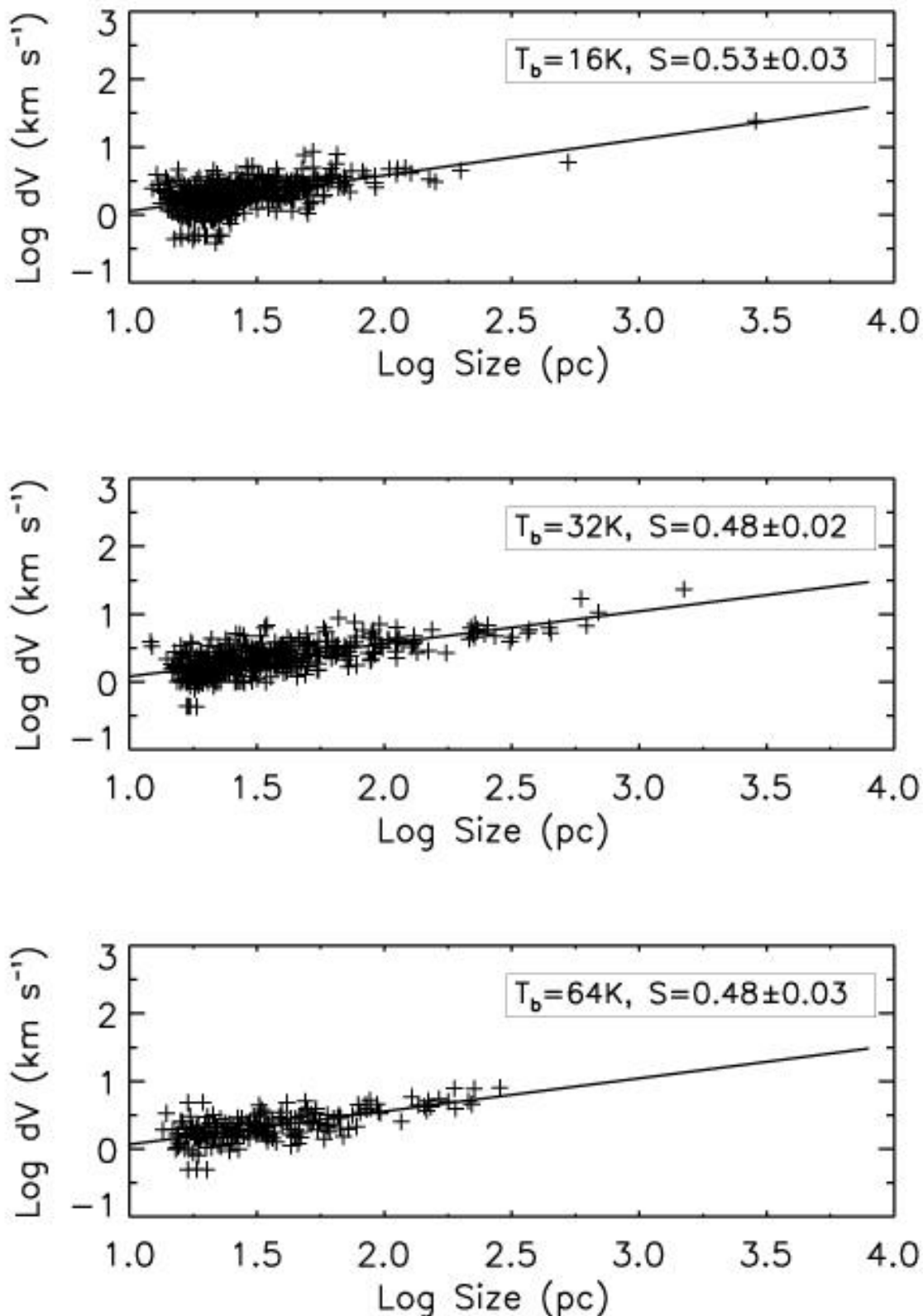


Fig. 6.— Size-Line Width Relation of the H I clouds in the entire region of the LMC for a given brightness temperature threshold.

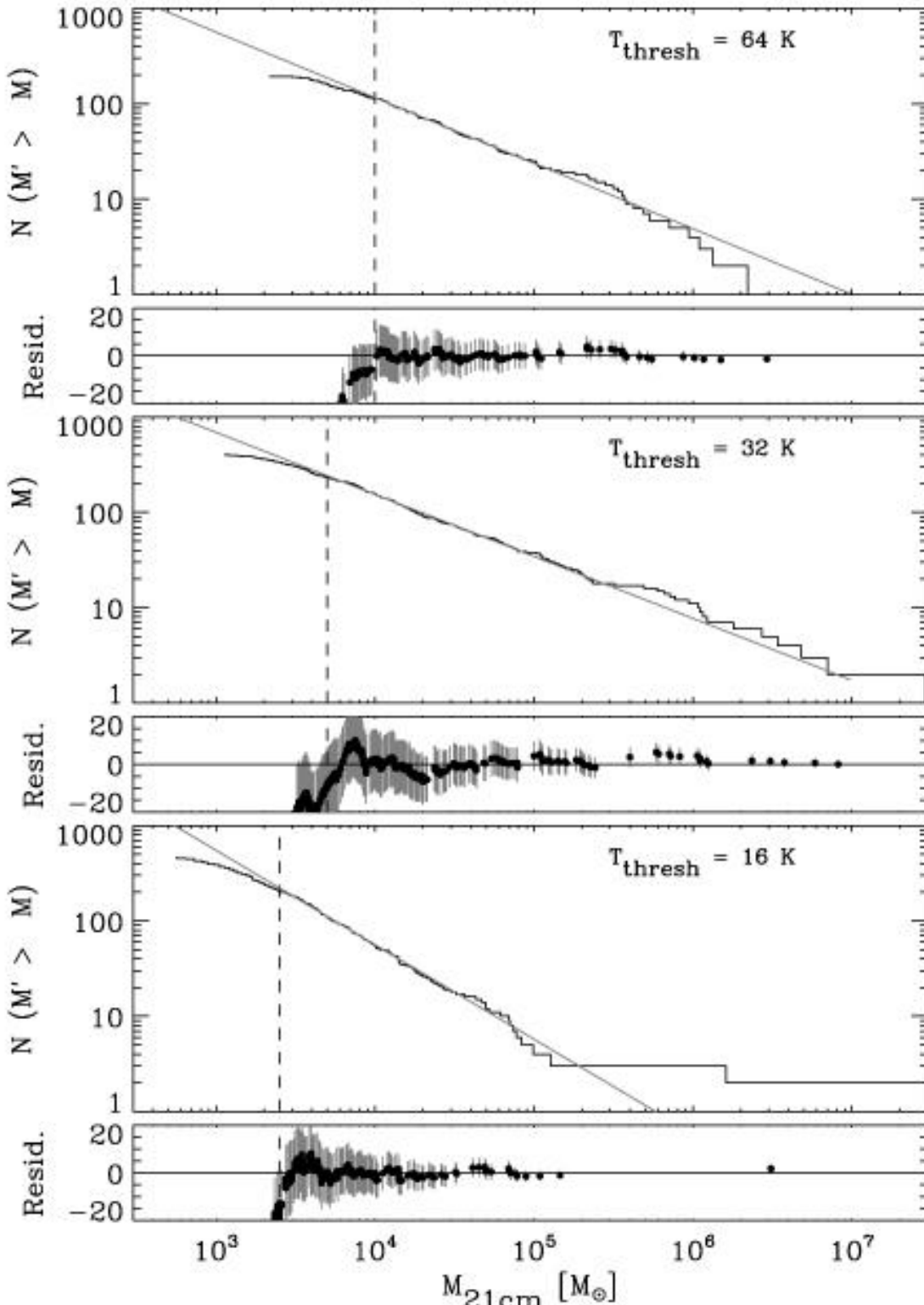


Fig. 7.— Cumulative mass distribution based on 21-cm luminosity for $T_{threshold} = 64, 32$, and 16 K in the top, middle and bottom large panels respectively. For each distribution, we fit a power law above masses of $10^4 M_\odot$ which is shown as a gray line. Parameters of the fit are given in Table 4. A vertical dashed line indicates the lower limit of clouds included in the fit. Small panels below each of the large panels represent the residuals of the fit in each case.

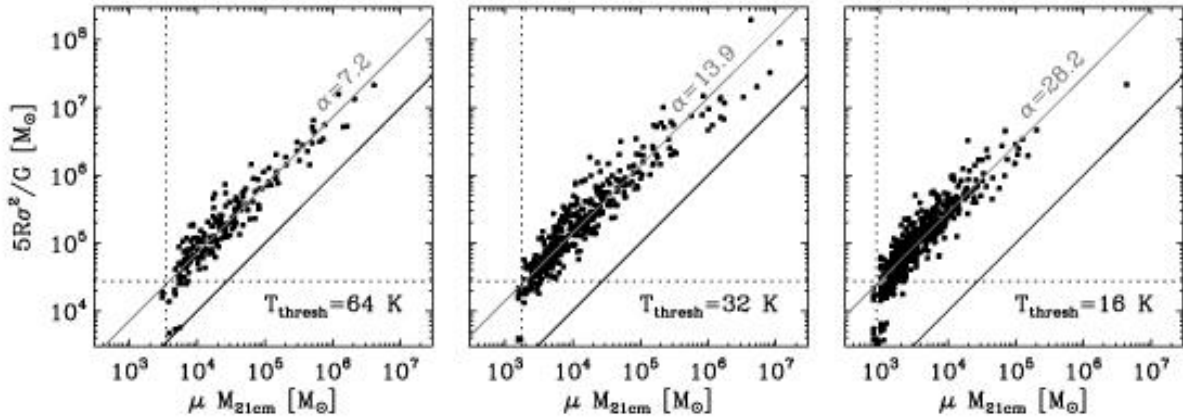


Fig. 8.— Comparison of luminous and dynamical mass estimates for clouds in each of the catalogs. The median virial parameter for each catalog is indicated with the gray diagonal line. The completeness limits for both quantities are shown as dotted lines.

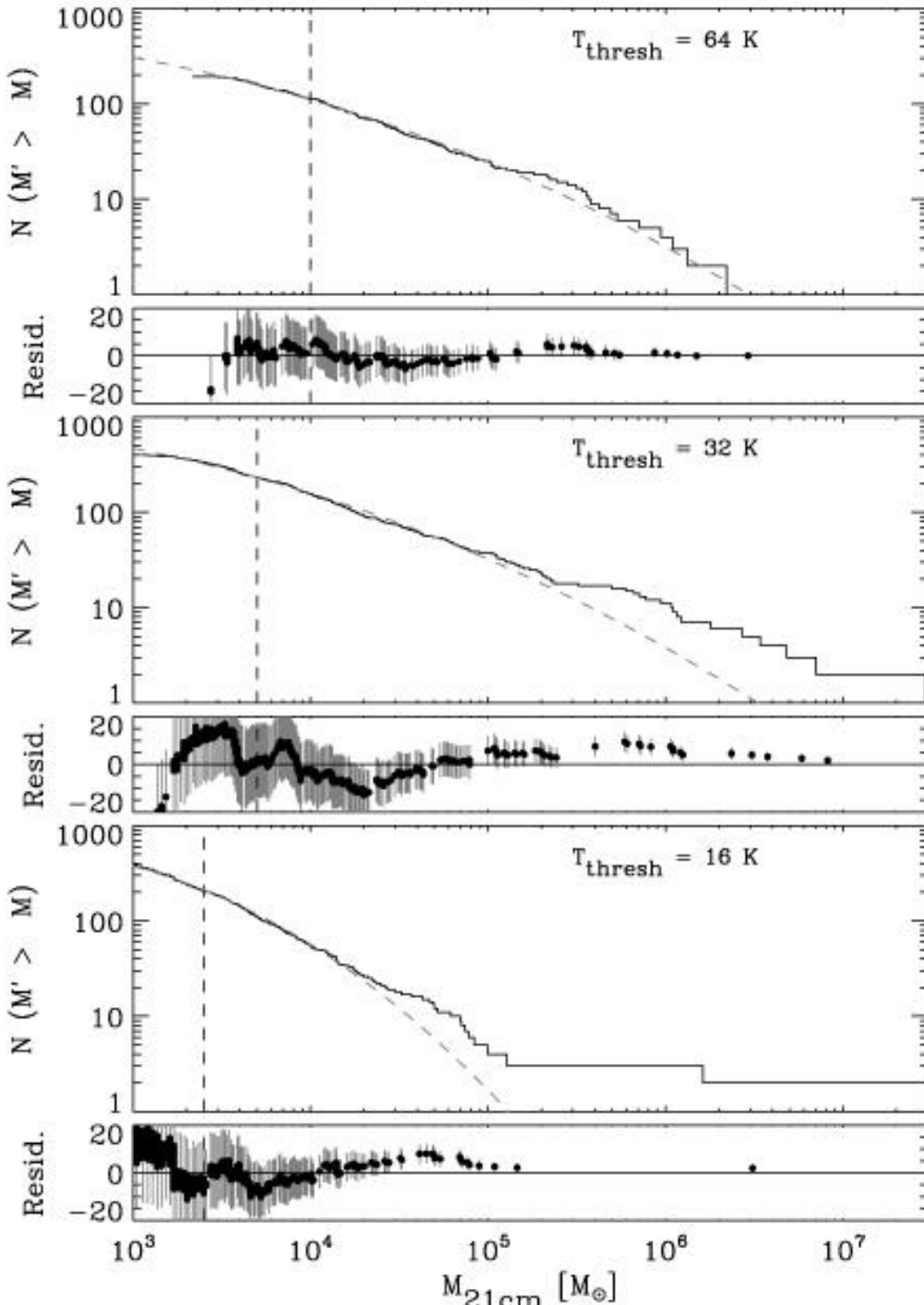


Fig. 9.— Cumulative mass distribution based on 21-cm luminosity for $T_{\text{threshold}} = 64, 32$, and 16 K in the top, middle and bottom large panels respectively. For each distribution, we fit a cumulative value function for a log-normal distribution above masses of $10^4 M_\odot$ which is shown as a gray line. Parameters of the fit are given in Table 4. A vertical dashed line indicates the lower limit of clouds included in the fit. Small panels below each of the large panels represent the residuals of the fit in each case.

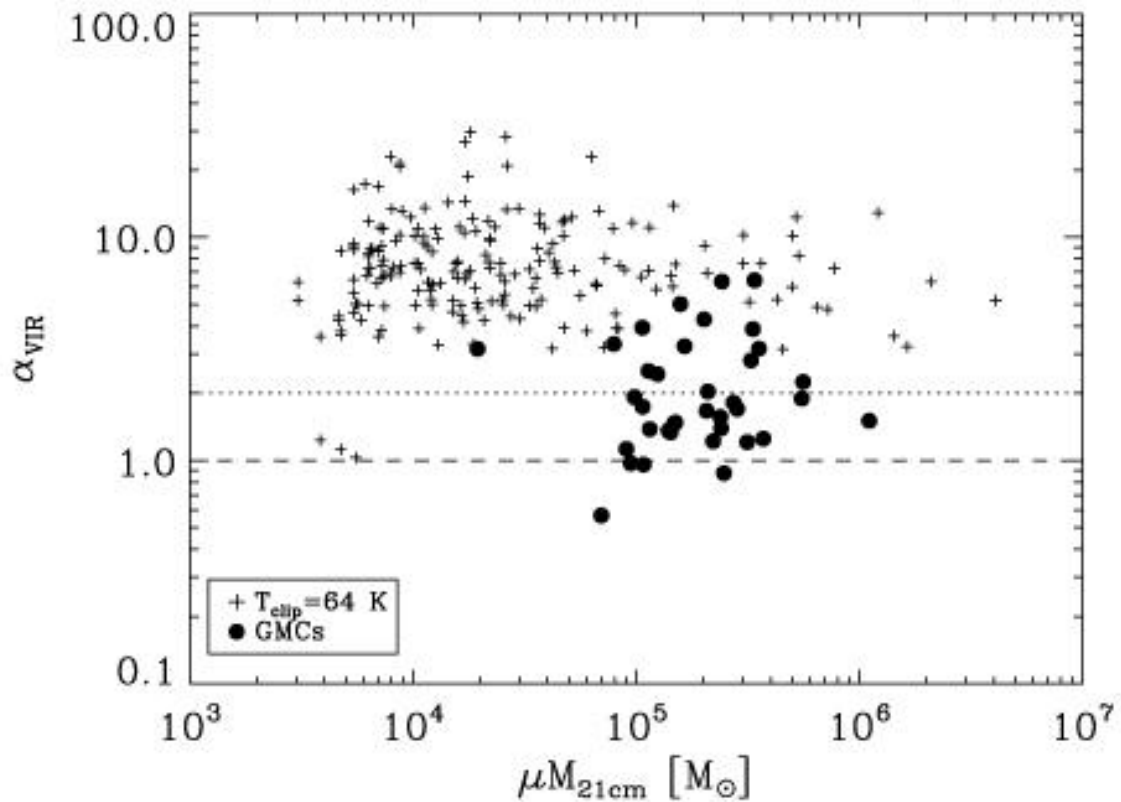


Fig. 10.— Virial parameter as a function of luminous mass for H I clouds and GMCs in the LMC. Neither type of clouds shows an obvious trend in the virial parameter with mass, but the mean virial parameters of the two systems are quite different.

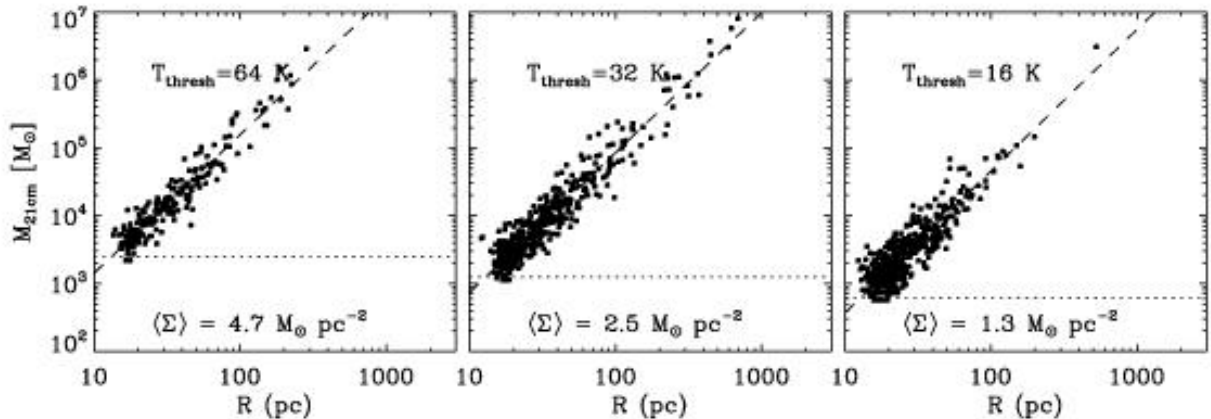


Fig. 11.— Radius-mass relationship for H I clouds in the LMC. The clouds follow the $M \propto R^2$ scaling expected from Larson’s laws based on a constant virial parameter and a size-line width relationship. Hence, the mean surface densities for all clouds are roughly constant and given in the panels of the Figure.

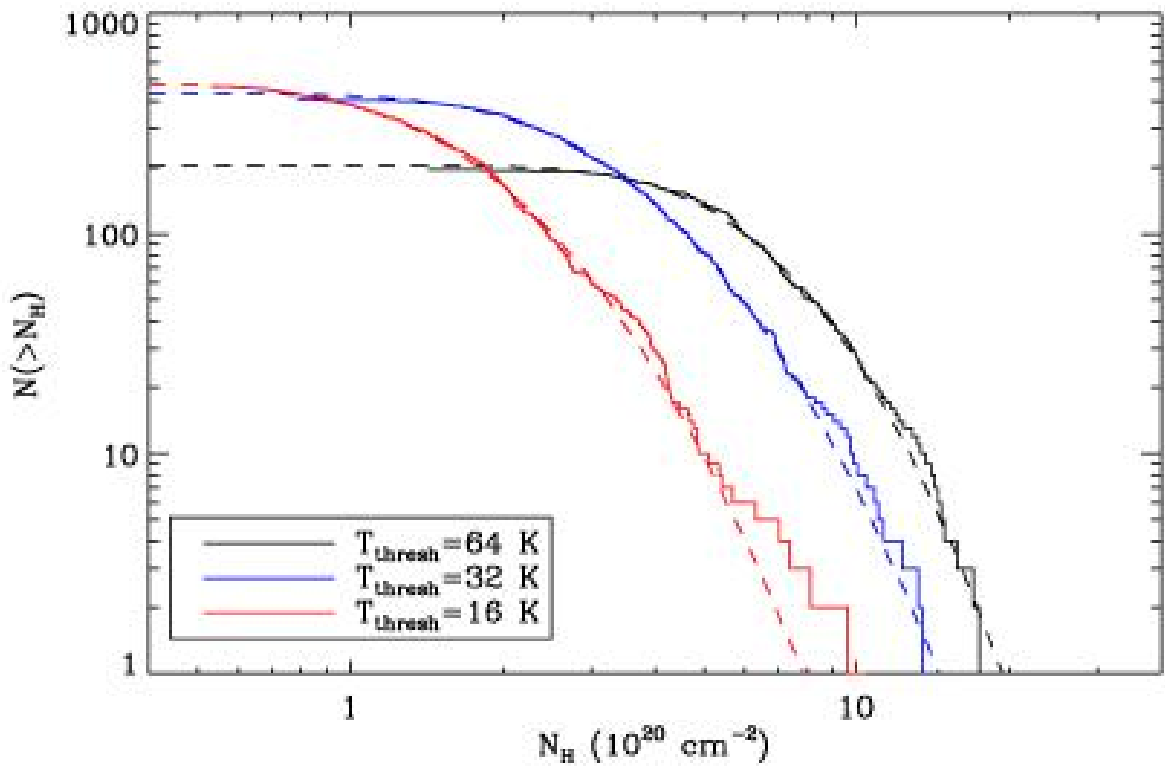


Fig. 12.— Cumulative distribution of H I column density. The observed distribution of column densities is shown as a solid line and a log-normal fit to the distribution is shown as a dashed line (see Table 5 for parameters). A power-law distribution would not reproduce the observed distribution.

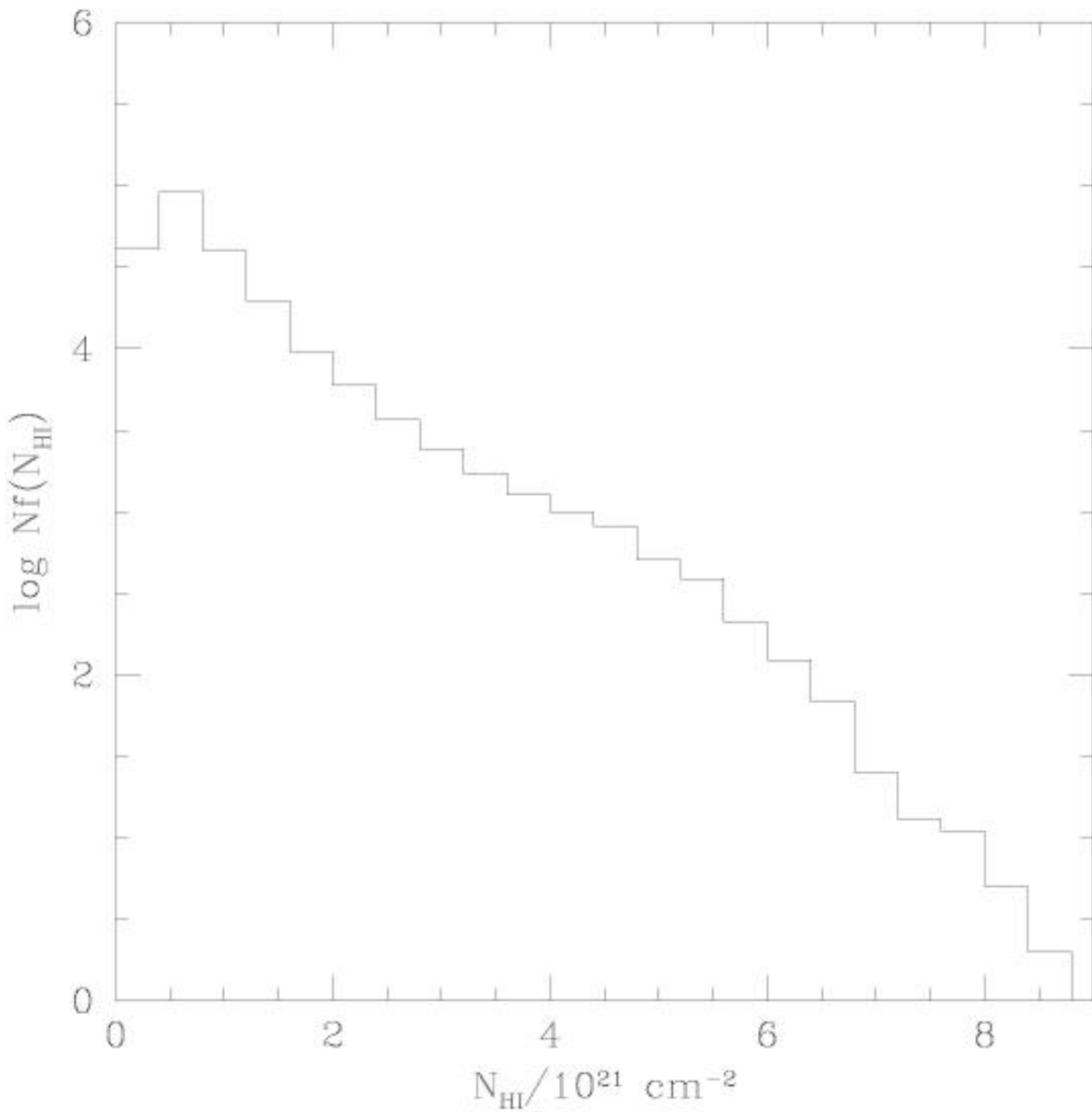


Fig. 13.— Observed column density distribution of H I along the line of sight is given.

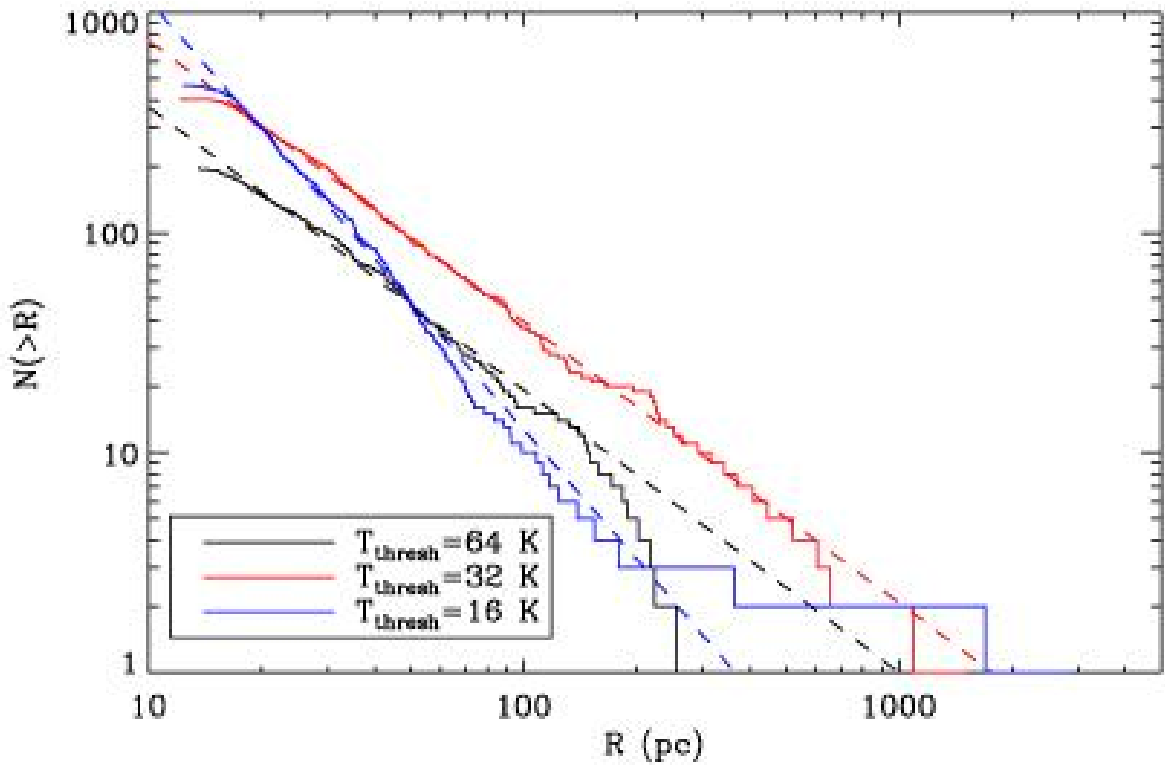


Fig. 14.— Size distribution of H I clouds. A power law form, $dN/dR \propto R^\beta$, is fit to the size spectrum for each catalog of clouds reproducing the observed shape of the distribution over the entire data range.

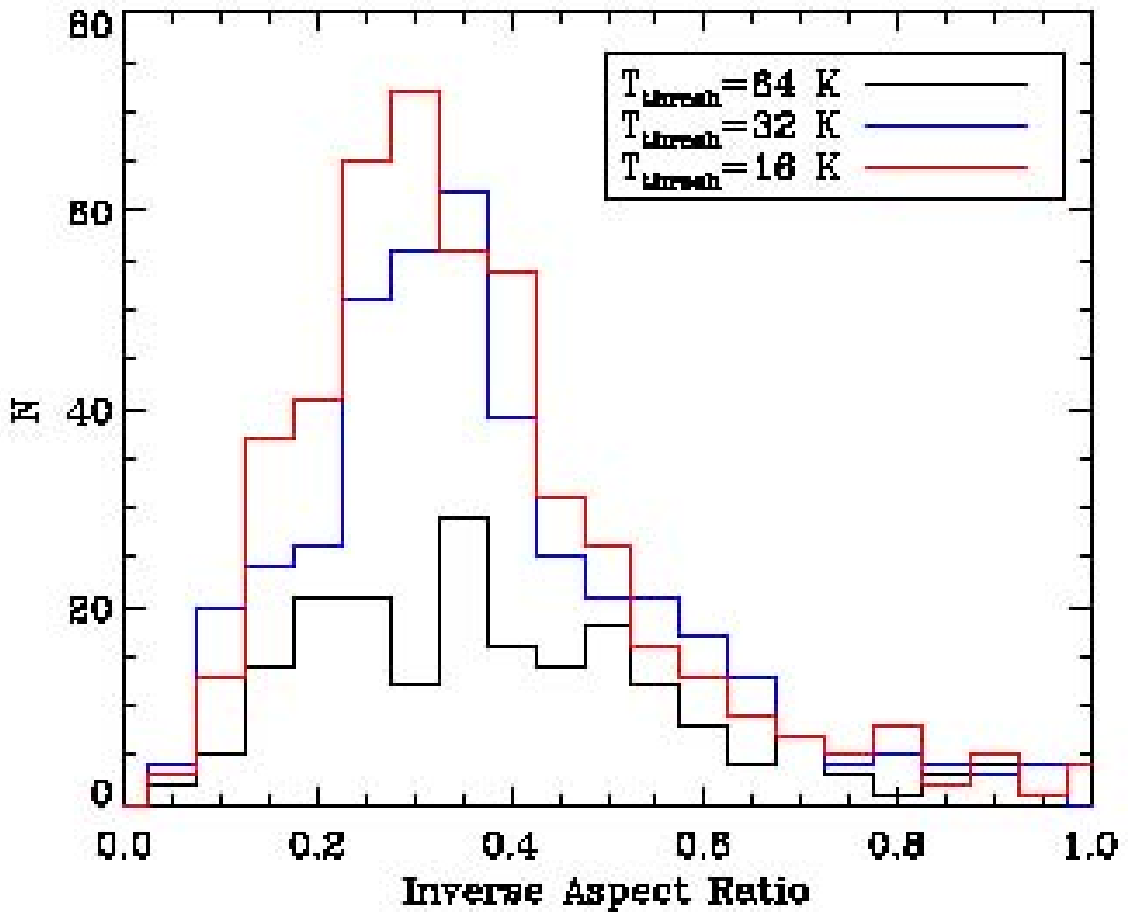


Fig. 15.— Histogram of inverse aspect ratio (minor/major) of the clouds. The peak distribution of inverse aspect ratio increases to 0.4 for the lower brightness temperature threshold.